8-2002

Determination of the Performance of a Prototype TurbX Engine

Kurt Erickson
University of Tennessee - Knoxville

To the Graduate Council:

I am submitting herewith a thesis written by Kurt Erickson entitled "Determination of the Performance of a Prototype TurbX Engine." I have examined the final electronic copy of this thesis for form and content and recommend that it be accepted in partial fulfillment of the requirements for the degree of Master of Science, with a major in Mechanical Engineering.

Rao V. Arimilli, Major Professor

We have read this thesis and recommend its acceptance:

Jeffrey W. Hodgson, Ming Zheng

Accepted for the Council:
Carolyn R. Hodges

Vice Provost and Dean of the Graduate School

(Original signatures are on file with official student records.)

To the Graduate Council:

I am submitting herewith a thesis written by Kurt Erickson entitled "Determination of the Performance of a Prototype TurbX Engine." I have examined the final electronic copy of this thesis for form and content and recommend that it be accepted in partial fulfillment of the requirements for the degree of Master of Science, with a major in Mechanical Engineering.

Rao V. Arimilli
Major Professor

We have read this thesis
and recommend its acceptance:

Jeffrey W. Hodgson

Ming Zheng

Accepted for the Council:

Dr. Anne Mayhew
Vice Provost and
Dean of Graduate Studies

(Original signatures are on file with official student records.)

DETERMINATION OF THE PEFORMANCE OF A PROTOTYPE TURBX ENGINE

A Thesis

Presented for the

Master of Science

Degree

The University of Tennessee, Knoxville

Kurt Erickson

August 2002

DEDICATION

I would like to dedicate this thesis to my dear wife

Nicole Erickson

for all her love, support and friendship

and to my parents

Lynn and JeNae Erickson

for their love and guidance

ACKNOWLEDGMENTS

I would like to express my deep gratitude to my major professor, Dr. Rao V. Arimilli, for his guidance throughout my research, technical advice, and most of all for his friendship and continuous suggestions, which went a long way in making the writing of this thesis a success. I would like to thank each of my other committee members, Dr. Jeffrey W. Hodgson and Dr. Ming Zheng, for their valuable suggestions and guidance during their review of this thesis.

In addition, I would like to thank Dr. James Conklin of ORNL for mentoring me throughout my research, for his continuous active support and for his valuable time spent teaching me real world experience and the importance of safety. I would also like to offer a special thanks to Dr. Michael A. Wilson, the inventor of TurbX™, for giving me the wonderful opportunity to gain hands on experience with new technology.

Finally, I would like to thank the following people for their assistance during my study at the University of Tennessee: Dr. Majid Keyhani, for his advice and also for his efforts finding me a graduate assistantship; Mr. Winston Holmes, for providing me a job; and The Mechanical and Aerospace Engineering and Engineering Science Department for supporting me financially throughout my graduate study.

ABSTRACT

The purpose of this study was to develop a testing procedure to measure the performance of a prototype TurbX™ engine. Dr. Michael A. Wilson invented a new concept internal combustion engine called TurbX™ and it is said to have higher efficiency and fuel economy compared to other engines. Theoretically, the TurbX™ engine cycle can be ideally represented by the Atkinson thermodynamic cycle with a continuous combustion process.

Oak Ridge National Laboratory and The University of Tennessee, Knoxville joined together to conduct tests to determine the performance of the TurbX™ engine. A total of 26 fired test runs were conducted to measure the TurbX™ engine performance characteristics as a function of speed. These were categorized into three separate cases based on rotational speed and the general quality or nature of combustion. The results from these tests clearly indicate that the TurbX™ engine produced no net output power for operational speeds up to 10,000 rpm. The temperature measurements indicated that for most of the runs there was sustained combustion. However, even in runs where satisfactory combustion was observed, measured gage pressure inside the combustion chamber never exceeded 15.5 kPa at 10,000 rpm. The lack of sufficient pressure rise inside the combustion chamber is indicative of excessive leakage through the rotor/stator clearance gap in the bladed section of the rotor and further development and research are needed to address this problem.

Based on the results and the experience gained through the testing procedure, several recommendations are made. For future testing, it is recommended that fuels with

high-flame velocities such as hydrogen or acetylene should be used, redesign the combustion chamber, reduce leakage through the air gap between the rotor and stators using a more direct approach to determine and adjust the size of the air gap, and improve the aerodynamic design of the stator expansion passages and rotor turbine blades.

TABLE OF CONTENTS

Chapter Page

1. INTRODUCTION 1
   - Introduction 1
   - TurbX™ Background 2

2. REVIEW OF LITERATURE 4

3. PROBLEM STATEMENT 11

4. DESCRIPTION OF ENGINE, TEST RIG AND TEST PROCEDURE 13
   - Components of TurbX™ 13
   - Operation of TurbX™ 15
   - Air Gap Associated with the Air Bearing 16
   - Experimental Test Setup 18
   - Air-driven Tests 21
   - Fired Tests 22
   - A Note About Project Deadline and Delays Associated with Engine Failures 26

5. RESULTS AND DISCUSSION 28

6. CONCLUSIONS AND RECOMMENDATIONS 49

LIST OF REFERENCES 51

APPENDICES 53
APPENDIX A 54
APPENDIX B 56

VITA 58

LIST OF TABLES

Table Page

1. Effect of air-bearing gap setting on average of peak gage pressures in kPa.....47

2. An abbreviated summary of fired-test results.....48

A.1 Premixed flame speeds of methane-air mixtures at atmospheric pressure 54

A.2 Tangential rotor velocity relative to methane flame velocities.....55

LIST OF FIGURES

Figure Page

1. Pressure-volume diagram of Atkinson, Otto and Brayton cycles having the same heat addition 4

2. Temperature-entropy diagram of Atkinson, Otto and Brayton cycles having the same heat addition....5

3. Comparison of the Atkinson, Otto and Brayton cycles' thermal efficiency....8

4. Diagram of the Holzwarth Gas Turbine....9

5. Schematic of three major components of the TurbX™ engine, a view showing details of Stator-1 14

6. Schematic of three major components of the TurbX™ engine, a view showing details of Stator-2 14

7. Gap control mechanism 16

8. The TurbX™ engine tested in the vertical-axis orientation....18

9. Schematic of the test rig used to test the TurbX™ engine 19

10. Barbour Stockwell air turbine and the TurbX™ engine....20

11. Schematic showing fired tests fuel flow control system and instrumentation....24

12. Case A, N = 1818, zero turns in from original gap setting....31

13. Case A, N = 2800, three turns in from original gap setting....31

14. Case A, N = 3888, three turns in from original gap setting 32

15. Case A, N = 4028, three turns in from original gap setting....32

16. Case B, N = 4690, three turns in from original gap setting....34

17. Case B, N = 4800, three turns in from original gap setting....34

18. Case B, N = 4902, three turns in from original gap setting....35

19. Case B, N = 5000, zero turns in form original gap setting 35
20. Case B, N = 5000, two turns in from original gap setting 36
21. Case B, N = 5160, three turns in from original gap setting 36
22. Case B, N = 5180-I, one turn in from original gap setting 37
23. Case B, N = 5180-II, one turn in from original gap setting 37
24. Case B, N = 5180, two turns in from original gap setting 38
25. Case B, N = 5300, zero turns in from original gap setting 38
26. Case B, N = 5374, three turns in from original gap setting 39
27. Case B, N = 5448, three turns in from original gap setting 39
28. Case B, N = 6000, three turns in from original gap setting 40
29. Case B, N = 6480, three turns in from original gap setting 40
30. Case B, N = 6880, three turns in from original gap setting 41
31. Case B, N = 6892, three turns in from original gap setting 41
32. Case B, N = 6902, three turns in from original gap setting 42
33. Case B, N = 7520, three turns in from original gap setting 42
34. Case C, N = 8200, three turns in from original gap setting 45
35. Case C, N = 8400, three turns in from original gap setting 45
36. Case C, N = 8460, three turns in from original gap setting 46
37. Case C, N = 9590, three turns in from original gap setting 46

LIST OF SYMBOLS AND ABBREVIATIONS

DC	Direct current
NTRC	National Transportation Research Center
ORNL	Oak Ridge National Laboratory
UTK	University of Tennessee, Knoxville
CH_4	Methane
c_p	Constant pressure specific heat, kJ/(kg·K)
c_v	Constant volume specific heat, kJ/(kg·K)
cm	Centimeter
in	Inches
kg	Kilogram
kPa	Kilopascals
kW	Kilowatt
lbs	Pounds
N	Rotational speed (rpm)
N-m	Newton meter
P	Gage pressure measured by the sensor
p	Specific pressure
psig	Pounds per square inch (gage pressure)
Q_R	Heat rejected (W)
Q_S	Heat supplied (W)
r	Compression ratio
rpm	Revolution per minute
s	Specific entropy
slpm	Standard liter per minute
T	Temperature
T^*	Maximum-to-minimum temperature ratio
v	Specific volume
°C	Degree Centigrade
%	Percentage
γ	Specific heat ratio
η	Thermal efficiency

CHAPTER 1
INTRODUCTION

Introduction

In recent years an emphasis has been placed on improving the overall efficiency of all forms of engines. With every new engine the goal of the designer is to achieve a high work output with greater efficiency. Dr. Michael A. Wilson invented a new concept internal combustion engine called TurbX™. TurbX™ is said to have higher efficiency and fuel economy compared to other engines. TurbX™ has a simpler design than reciprocating engines in that it requires far fewer moving parts resulting in potentially lower manufacturing, maintenance and repair costs. This engine has the potential to compete with power generating devices in several transportation and stationary power generation applications.

TurbX™ could benefit many different markets including aero-propulsion, automobiles, and electric-power utility companies. A slight increase in engine efficiency would have a tremendous impact financially and environmentally.

Theoretically, the TurbX™ engine cycle can be represented by the Atkinson thermodynamic cycle with a continuous combustion process. The Atkinson cycle has higher thermal efficiency than the Otto cycle (automobile gasoline engines) and the Brayton cycle (gas turbines) for a given volumetric ratio. Reciprocating piston engines operating on the Otto cycle can be modified to operate on the Atkinson cycle, but geometric complexities and added costs have prevented much development of engines operating on this cycle. The goal of the TurbX™ engine is to implement the thermodynamic Atkinson cycle to increase efficiency of gas turbine engines.

The efficiency of current gas turbine engines is directly related to operating temperatures. In gas turbine engines the turbine is directly exposed to high-pressure high-temperature conditions and these conditions are limited by material considerations such as creep and fatigue. The turbine is continuously exposed to these severe conditions during the operation of the engine. The mechanical part (rotor) in the TurbX™ engine is exposed to high-pressure high-temperature conditions in the combustion chamber for only a fractional portion of each rotation of the rotor. Therefore, the mean temperature experienced by the rotor is lower when compared to conventional turbine engines. This would allow higher temperatures to be utilized in the TurbX™ combustion chamber resulting in greater engine efficiency.

The simple design of the TurbX™ engine allows it to be run with far fewer devices and does not require the many parts associated with reciprocating engines, such as pistons, crank shafts, valves, gears, chains, pumps, etc. TurbX™ does not include these additional parts, which decrease the overall engine efficiency. Furthermore, the simple design of TurbX™ would lower manufacturing, maintenance and repair costs.

TurbX™ Background

Dr. Michael A. Wilson, the inventor of TurbX™, began working on this new concept engine in 1983. He further developed the concept in 1995. In 1997 the proof of the concept was completed. The preliminary prototype engine fabrication was completed in 1998. United States Patent Number 5,966,927 [1] was issued to Dr. Michael Wilson in 1999 followed by a second patent, United States Patent Number 6,105,369 [2], issued in 2000. Following the two patents, Dr. Wilson approached several companies and

organizations to try to move this new technology forward. In that process it became clear that the test results of the actual performance of the prototype engine, preferably by a third party, were essential to justify further developmental activity related to this engine.

This new concept engine caught the attention of several engineers and companies. Oak Ridge National Laboratory (ORNL) and the University of Tennessee Knoxville (UTK) were especially interested in the concept. With small funding from the Tennessee State Energy Partnership Program, they decided to collaborate in a joint effort to conduct tests, to determine the performance of the engine at the National Transportation Research Center (NTRC) located in Knoxville, Tennessee. The NTRC is a joint effort involving ORNL and UTK.

CHAPTER 2
REVIEW OF LITERATURE

The TurbX™ engine can be represented ideally by the theoretical Atkinson thermodynamic cycle [3]. The Atkinson cycle is represented by 1-2-3-4-1 as shown in Figure 1 on the *p*-*v* diagram and Figure 2 on the *T*-*s* diagram. The Atkinson cycle is similar to the Otto cycle with the difference that the rejection of heat in the Atkinson cycle is at constant-pressure instead of at constant-volume as in the Otto cycle. The Otto cycle is represented by 1-2-3-4″-1. Inspection of Figure 1 shows that the expansion process 3-4″ has not proceeded to the lowest possible pressure, resulting in dissipation of available energy. By increasing the expansion or power stroke to the lowest pressure and exhausting gases to atmospheric conditions, while maintaining the same quantity of heat added, the thermal efficiency of the Atkinson cycle is greater than that of the Otto cycle because of the increased amount of net work indicated by the area 4″-4-1-4″ [4], [5].

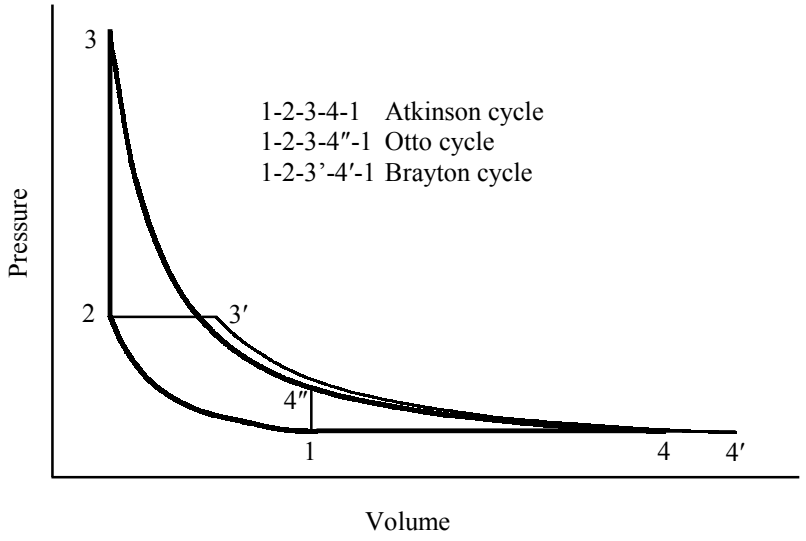

Figure 1. Pressure-volume diagram of Atkinson, Otto and Brayton cycles having the same heat addition

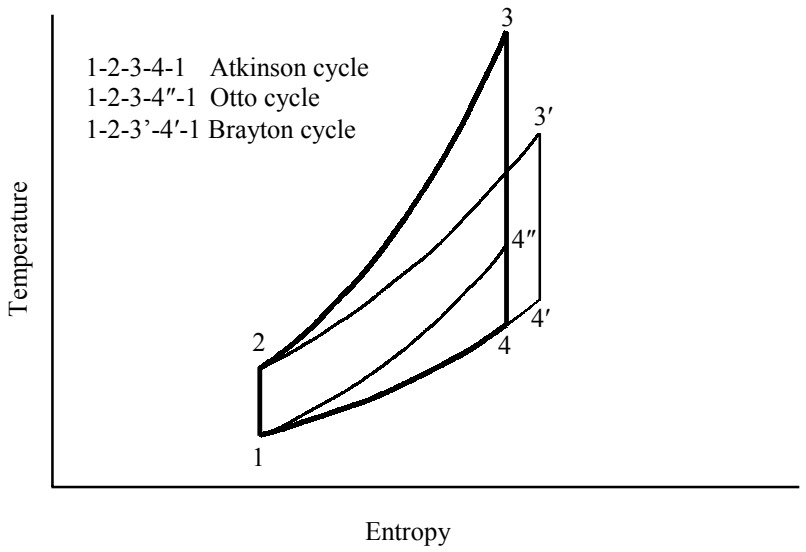

Figure 2. Temperature-entropy diagram of Atkinson, Otto and Brayton cycles having the same heat addition

The Atkinson cycle is also similar to the Brayton cycle with the difference that the addition of heat in the Atkinson cycle is at constant-volume instead of at constant-pressure as in the Brayton cycle. The Brayton cycle is represented by 1-2-3′-4′-1 in Figures 1 and 2. Inspection of Figure 1 shows that for the same quantity of heat added in the constant-volume process rather than constant-pressure process, the thermal efficiency is increased because the net work area corresponding to 1-2-3-4-1 (Atkinson cycle) is greater than the net work area corresponding to 1-2-3′-4′-1 (Brayton cycle).

The specific volume ratio (v_1/v_2) is used as the basis for comparing the thermal efficiencies of the Otto cycle and Brayton cycle to the Atkinson cycle. For the Otto cycle, v_1/v_2 is referred to as the compression ratio (r). The thermal efficiencies of the three cycles are compared for the same volume ratio to show which cycle is more thermally efficient.

The thermal efficiency of the Atkinson cycle 1-2-3-4-1 can be written as

$$\eta_{\text{Atkinson}} = \frac{Q_S - Q_R}{Q_S} \tag{2.1}$$

Considering constant volume process 2-3 and constant-pressure process 4-1, the heat supplied and the heat rejected can be written (for ideal gas behavior with constant specific heats) as

$$Q_S = mc_v(T_3 - T_2) \tag{2.2}$$

$$Q_R = mc_p(T_4 - T_1) \tag{2.3}$$

Substituting into the expression for η_{Atkinson},

$$\eta_{\text{Atkinson}} = \frac{mc_v(T_3 - T_2) - mc_p(T_4 - T_1)}{mc_v(T_3 - T_2)} = 1 - \gamma\left(\frac{T_4 - T_1}{T_3 - T_2}\right) \tag{2.4}$$

For the isentropic compression process 1-2, the temperature ratio (T_2/T_1) can be expressed in terms of the volume ratio as follows

$$\frac{T_2}{T_1} = \left(\frac{v_1}{v_2}\right)^{\gamma-1} = r^{\gamma-1} \tag{2.5}$$

Rearranging and substituting one gets the following

$$\eta_{\text{Atkinson}} = 1 - \gamma\left[\frac{T_1\left(\frac{T_4}{T_1} - 1\right)}{T_2\left(\frac{T_3}{T_2} - 1\right)}\right] = 1 - \gamma\left[\frac{1}{\left(\frac{v_1}{v_2}\right)^{\gamma-1}}\left(\frac{\frac{T_4}{T_1} - 1}{\frac{T_3}{T_2} - 1}\right)\right] \tag{2.6}$$

Using the ideal gas equation of state for the constant-volume process 2-3, isentropic relations for the compression process 1-2 and the expansion process 3-4, and constant pressure for the process 4-1 that completes the cycle results in the following

$$\frac{T_3}{T_2} = \frac{p_3}{p_2} = \left(\frac{p_3}{p_4} \times \frac{p_4}{p_2}\right) = \left(\frac{p_3}{p_4} \times \frac{p_1}{p_2}\right) \tag{2.7}$$

$$\frac{T_3}{T_2} = \left(\frac{v_4}{v_3} \times \frac{v_2}{v_1} \right)^{\gamma} = \left(\frac{v_4}{v_1} \right)^{\gamma} = \left(\frac{T_4}{T_1} \right)^{\gamma} \tag{2.8}$$

The temperatures T_1 and T_3 can be expressed in terms of the maximum-to-minimum temperature ratio $T_3/T_1 = T^*$. Therefore,

$$\frac{T_3}{T_2} = \frac{T^*}{\left(\frac{v_1}{v_2} \right)^{\gamma-1}} \tag{2.9}$$

$$\eta_{\text{Atkinson}} = 1 - \gamma \left[\frac{\left(T^*\right)^{\frac{1}{\gamma}} \left(\frac{v_1}{v_2} \right)^{\frac{1-\gamma}{\gamma}} - 1}{T^* - \left(\frac{v_1}{v_2} \right)^{\gamma-1}} \right] \tag{2.10}$$

Note that thermal efficiency of the Atkinson cycle is a function of specific volume ratio (v_1/v_2), the ratio of specific heats (γ) and the maximum-to-minimum temperature ratio (T^*).

The efficiency of the Otto cycle is given by

$$\eta_{\text{Otto}} = 1 - \frac{1}{r^{\gamma-1}} \tag{2.11}$$

Note that the thermal efficiency of Otto cycle is a function of compression ratio (r) and the ratio of specific heats (γ) only.

The efficiency of the Brayton cycle is given by

$$\eta_{\text{Brayton}} = 1 - \frac{1}{\left(\frac{p_2}{p_1} \right)^{\frac{\gamma-1}{\gamma}}} = 1 - \frac{1}{\left(\frac{v_1}{v_2} \right)^{\gamma-1}} \tag{2.12}$$

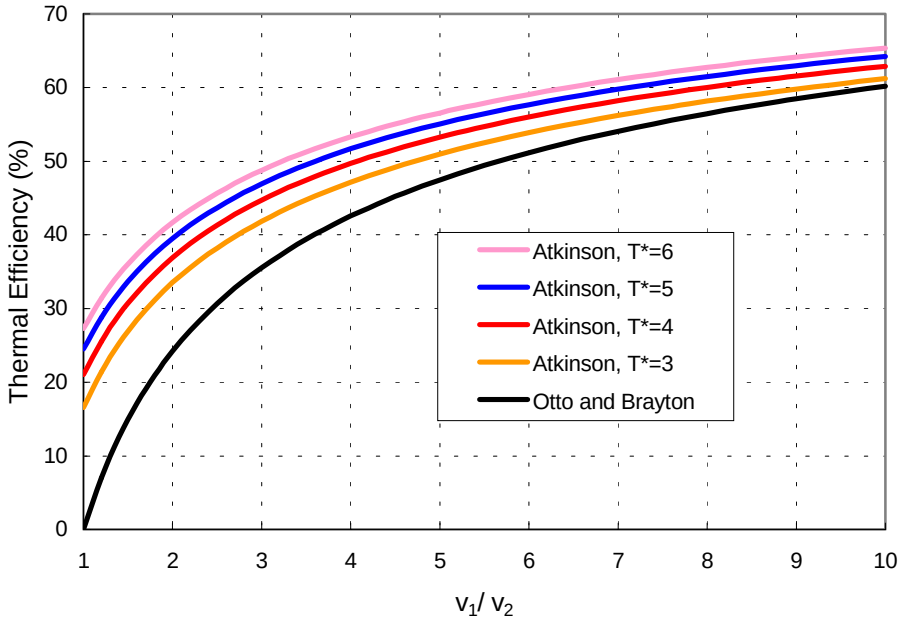

Figure 3. Comparison of the Atkinson, Otto and Brayton cycles' thermal efficiency

For a given specific volume ratio, the Otto cycle has the same thermal efficiency as the Brayton cycle. Figure 3 shows the thermal efficiency for each cycle as a function of specific volume ratio. Assuming air as the working fluid, the ratio of specific heats $\gamma = 1.4$.

Figure 3 illustrates the Atkinson cycle has greater thermal efficiency than the Brayton cycle and the Otto cycle, especially at low specific volume ratios. Also shown in Figure 3, is that the thermal efficiency of the Atkinson cycle increases with increasing maximum-to-minimum temperature ratio (T^*) for all specific volume ratios.

A recent study on increasing gas turbine efficiency accomplished by constant-volume combustion is presented by Venturini and Varella [6]. They analyzed a small gas turbine working under a cycle proposed by Dr. Holzwarth and compared it with gas turbines operating under constant-pressure combustion (Brayton cycle).

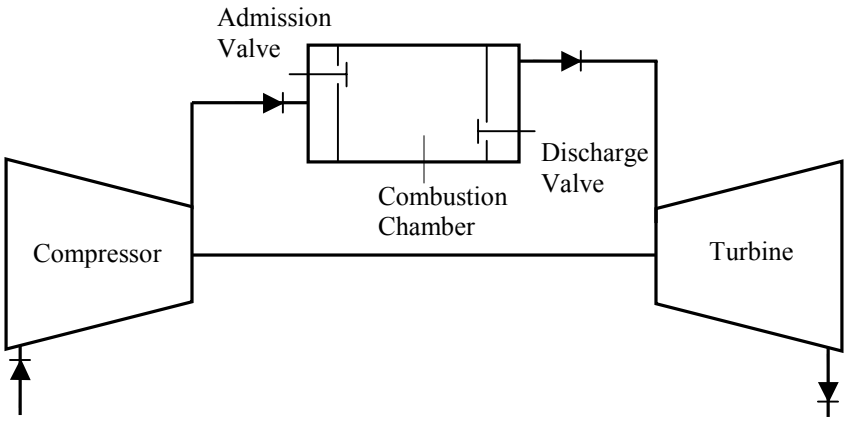

Figure 4. Diagram of the Holzwarth Gas Turbine

In the early 20th century Dr. Holzwarth of Germany started working on what was later known as the explosion gas turbine. In the Holzwarth engine, the compressor introduced air and fuel into a constant-volume combustion chamber. Figure 4 shows a diagram of a gas turbine operating on the Holzwarth cycle. When the air-fuel mixture is ignited, the pressure of the gases increase immediately after the admission valve closes, reaching a maximum in the combustion chamber from which the gases are discharged through a valve and allowed to expand in the turbine.

When a gas turbine operates on the Holzwarth cycle, the compressor and turbine are subjected to periodic temperature and pressure variations. Venturini and Varella performed a simplified analysis of the Holzwarth cycle based on quasi-steady thermodynamic analysis. The actual performance parameters of the turbine and compressor, obtained from their operation performance maps, are also incorporated into this analysis.

The thermal efficiency for the Holzwarth cycle was shown to be significantly higher than the gas turbine operating under the Brayton cycle especially at low

compressor pressure ratios (specific volume ratios). Therefore, the Holzwarth gas turbine has advantages over the Brayton cycle, and has the potential for the development of more efficient gas turbines using smaller compressors. The cycle proposed by Holzwarth is equivalent to the Atkinson cycle, both having heat addition in constant-volume processes. It is possible to run the Holzwarth cycle at low-pressure ratios by using either a blower or a high efficiency low-pressure ratio compressor to charge the explosion turbine. For a pressure ratio of one (compression ratio of one), fuel burned at atmospheric pressure inside the combustion chamber is sufficient to raise the pressure and create power as the gases expand. However, one cannot avoid the use of a blower or a compressor, as there is no suction pressure available in the combustion chamber. In contrast to this, the tested prototype TurbX™ engine does not have a blower or compressor because it has the ability to create suction at the air inlet ports and could produce power at a pressure ratio of one after it is started by external means. It should be pointed out that at a pressure ratio of one the Atkinson cycle reverts to the Lenoir cycle, which predates the Otto cycle.

CHAPTER 3
PROBLEM STATEMENT

The TurbX™ engine has never been tested and therefore the engine parameters to measure along with their estimated ranges were identified. Choosing the appropriate instrumentation was important for accurately measuring the performance of the engine within budget and time limitations. The data was collected using Lab View, a data acquisition software program by National Instruments. The primary parameters measured included: output shaft torque and speed, volumetric flow rates of inlet air and fuel, combustion chamber temperatures and gage pressure, stator temperatures at selected locations, gage pressure and temperature in the last stator expansion chamber, exhaust temperature and gap between the rotor and the two stators.

In the test plan developed, the need for two distinct tests were recognized, namely, fueled and un-fueled tests. The un-fueled test is also referred to as the air-driven test and the fueled test is also referred to as the fired test. First, the air-driven test was conducted using compressed air to drive the engine. Compressed air was fed into the spark plug port and allowed to expand in the TurbX™ engine stator expansion passages, and spin the shaft to deliver torque. Compressed technical grade methane (98% CH_4) was the fuel used for the fired test.

The air-driven test was conducted to gain operational experience with the TurbX™ engine without having to deal with the complexities associated with fuel handling and combustion involved in the fired tests. Operational experience from the air-driven test provided valuable information about the effectiveness of the air bearing and

the effectiveness of the mechanism for adjusting the air gap to small enough values to reduce leakage losses. Some engineers, who previously reviewed the engine concept, consider these issues to be problematic with the TurbX™ engine. The results for the air-driven tests will be documented in more detail and presented in a thesis by Frederick Mottley.

The purpose of the fired test, fueled by methane, was to measure the engine performance characteristics as a function of speed. The characteristics of interest are the output torque, fuel flow rate and other relevant thermodynamic parameters including the combustion chamber gage pressure and temperature. The results for the fired tests are presented in this thesis.

CHAPTER 4

DESCRIPTION OF ENGINE, TEST RIG AND TEST PROCEDURE

Components of TurbX™

The prototype TurbX™ engine was designed by Dr. Michael A. Wilson to produce 15 kW of power at a design speed of 20,000 rpm. The TurbX™ engine is compact and light weight relative to other engines producing similar amount of power, having dimensions of 0.1905 m (7.5 in.) square by 0.0381 m (1.5 in.) thick, weighing only about 9.072 kg (20 lbs.). The components that make up TurbX™ are two stators, a rotor, a casing that keeps the rotor positioned in between the two stators and an output drive shaft [1,2]. The engine components are all made of invar. A solid model of the three major components of the TurbX™ engine, two stators and rotor, was created in Solid Works® commercial computer software [7] and is shown in Figures 5 and 6.

The rotor, located in between the two stators, is the only rotating component; all the other components are stationary. The rotor is supported between the two stators by an air bearing which provides a thin film of pressurized air. The air bearing allows the rotor to rotate nearly frictionless for any rotational speed. The two faces of the rotor and the interfacing surfaces of the two stators are machined to minimize the possibility of surface-to-surface contact while the rotor is rotating.

The thickness of the thin pressurized layer of air between the rotor and the two stators is referred to as *the air gap*, or simply *the gap*. The threading on the inside of the casing and the perimeter of the two stators is such that by rotating both stators in the same angular direction, the two stators move either further away or closer to the rotor.

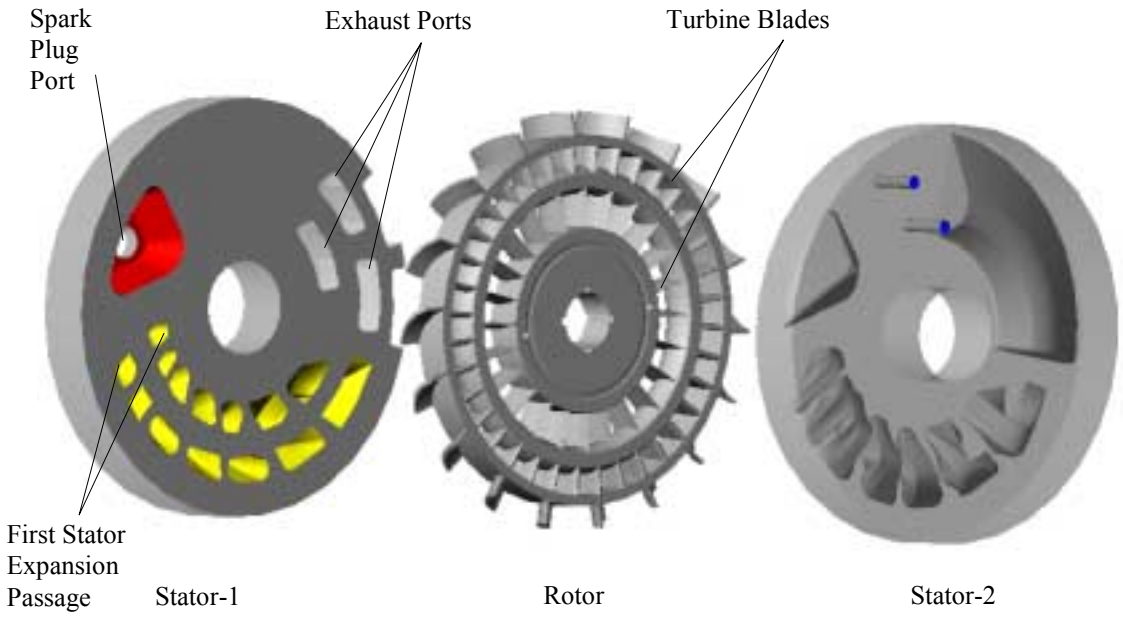

Figure 5. Schematic of three major components of the TurbX™ engine, a view showing details of Stator-1

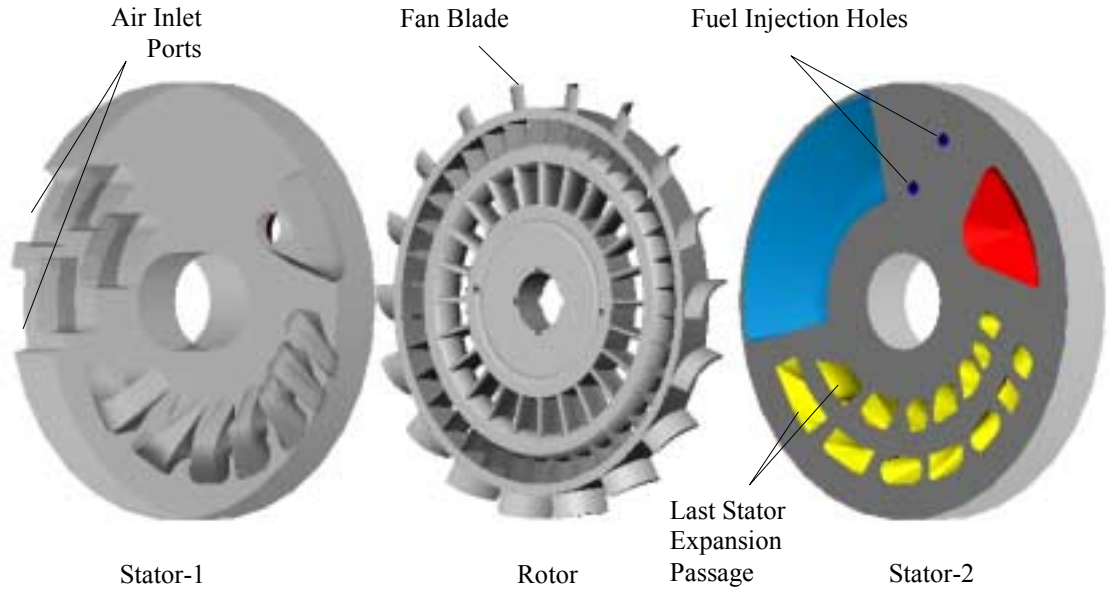

Figure 6. Schematic of three major components of the TurbX™ engine, a view showing details of Stator-2

Operation of TurbX™

The entire suction, combustion and expansion processes operate within the three major components that make up the TurbX™ engine, shown in Figures 5 and 6. Air enters the engine through two-air inlet ports located on stator-1 and is swept into the engine by fan blades that are on to the outer periphery of the rotor. Fuel is injected through two small holes located on stator-2. The air and fuel mix in the trapped region between the turbine blades. The trapped air-fuel mixture is swept between the stators to the combustion chamber (highlighted in red) where ignition is accomplished by a spark-plug igniter located in stator-1. The rotor carries the burning air-fuel mixture to the first stator expansion passage (highlighted in yellow). The burning air-fuel mixture trapped in the space between adjacent blades of the rotor continues to burn without expansion as it moves from the combustion chamber to the first stator expansion passage. Therefore, the heat addition can be considered to be at constant volume.

As the high-temperature high-pressure gas passes over the first stator expansion passage, the available energy is partially converted into kinetic energy. The jet of gas accelerates through the first stator expansion passage making an approximately 180° turn from which it reenters the rotor at high velocity hitting the turbine blades. The turbine blades convert the kinetic energy of the moving gas into work. The gas again enters another expansion chamber, only this time located on the other stator where it undergoes further expansion. The gas continues to expand as it spirals in the circumferential direction entering each stator a total of seven times before exhausting out of the engine through the exhaust ports located on stator-1.

Air Gap Associated with the Air Bearing

A lever arm mechanism shown in Figure 7 is used to adjust the size of the air gap. Two lever arms are attached, one to the outside of each stator. The two lever arms are connected in such a way that both stators are allowed to rotate together in the same angular direction. Adjusting the gap is accomplished by rotating the nut that is attached to the bolt centered between the two lever arms. From the geometric details of the gap control mechanism, for each complete revolution of the nut; the gap on each side of the rotor would change by approximately 0.0000043 m (0.00017 in.).

To initialize the air gap, the gap was set at a relatively large value and compressed air supplied to the air bearing was turned on with the engine turned off. By freely rotating the output shaft by hand while simultaneously turning the nut, the two stators were rotated to bring them closer to the rotor until a slight rotational resistance in the

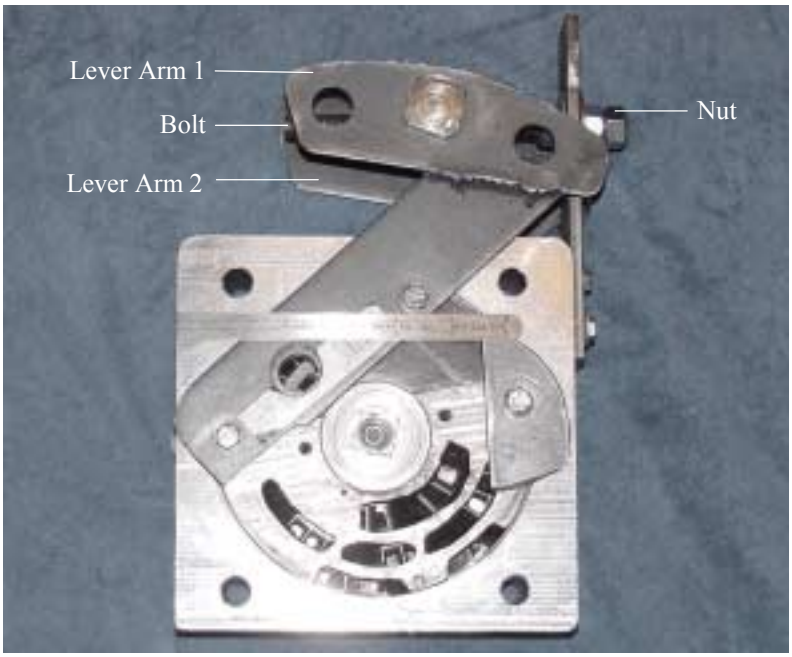

Figure 7. Gap control mechanism

output shaft is encountered, indicating contact with the rotor. At this position, the gap is considered to have zero thickness. From this position, the nut is rotated eight full turns in the opposite direction to allow the two stators to move further apart. The nut is then rotated once again in the opposite direction four full turns, for the runs reported in this study, to bring the stators closer. The air gap corresponding to this position of the stators is called the *original gap*. However, the backlash in the control mechanism made it difficult to determine the exact gap width corresponding to this original gap.

To determine the effect of the gap, tests were conducted at four different values of gaps starting with the widest gap (the original gap also referred to as *zero turns*) and proceeding to the smallest gap by turning the nut (in the same direction and without backlash) one full turn at a time up to a total of three turns. With less than 24 hours available to complete the fuel-fired engine tests, it was important to finish as much of the testing as possible. With this limited amount of time, risking the danger of freezing the rotor between the stators with the gap setting any smaller than the value associated with three turns, was not an option. The gaps used are referred to in this report as *zero turns*, *one turn*, *two turns* and *three turns*.

The first set of fired test runs were conducted with the original gap. The original gap, as already indicated, is called *zero turns* of the nut, which represents the widest gap. In the succeeding sets of runs, the gap size was decreased in steps by turning the nut one complete turn at a time for a total of three turns. Thus, three turns of the nut represents the narrowest gap.

Experimental Test Setup

To test the TurbX™ engine up to its design speed of 20,000 rpm, a test rig was designed, fabricated and equipped with appropriate instruments by Frederick Mottley, a UTK graduate student. Fred was responsible for the design and construction of the test rig as part of his thesis project and also to perform the air-driven tests. The engine is capable of operating with its axis of rotation either horizontal or vertical, but was tested in a vertical-axis orientation as shown in Figure 8.

The test rig used to test the TurbX™ engine is shown in Figure 9. TurbX™ was suspended from a four-inch diameter steel plate with a metallic frame using slotted channels. The frame supports the TurbX™ engine and the Magtrol torque meter. A type TM 207 torque transducer by Vibro-Meter instrumentation division of Magtrol Corporation was used for torque and speed measurements over a broad range for both air-driven and fired tests. The transducer outputs a 0 to ±5V DC electrical signal for a 0-10 N-m torque for speeds up to 50,000 rpm.

Figure 8. The TurbX™ engine tested in the vertical-axis orientation

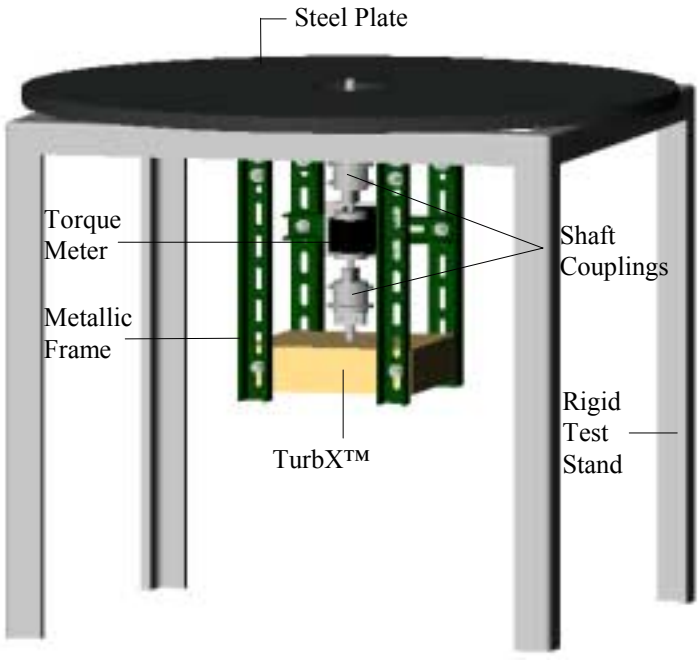

Figure 9. Schematic of the test rig used to test the TurbX™ engine

A Barbour Stockwell air turbine (not shown in Figure 9) was placed on top of the steel plate and used as a dynamometer for both air-driven and fired tests. The Barbour Stockwell air turbine, containment shield and rigid test stand were all made available by NTRC to test TurbX™. To keep the project within budget, this equipment had to be used and this is the basis for testing TurbX™ in the vertical-axis orientation. The containment shield fit around the metallic frame and provided safety during the operation of TurbX™ during fired tests.

The Barbour Stockwell air turbine output shaft is coupled to one shaft of the Magtrol torque meter, and the other shaft is coupled to the output shaft of the TurbX™ engine. The Magtrol torque meter was mounted in-line between the output shafts of the Barbour Stockwell air turbine and the TurbX™ engine. Flexible shaft couplings, Thomas Miniature Couplings Model Number 62 CBC, were used to safely transmit torque

between TurbX™, torque meter and air turbine shafts by compensating for undetected shaft misalignment.

The Barbour Stockwell air turbine shown in Figure 10 has two compressed-air supply ports, referred to as primary and secondary ports. Supplying air to the primary port causes the air turbine to rotate clockwise (looking down on it) and supplying air to the secondary port causes in the air turbine to rotate counter-clockwise. Air is supplied to only one port at any given time. The rotational speed of the air turbine was regulated by a manually operated gate-valve.

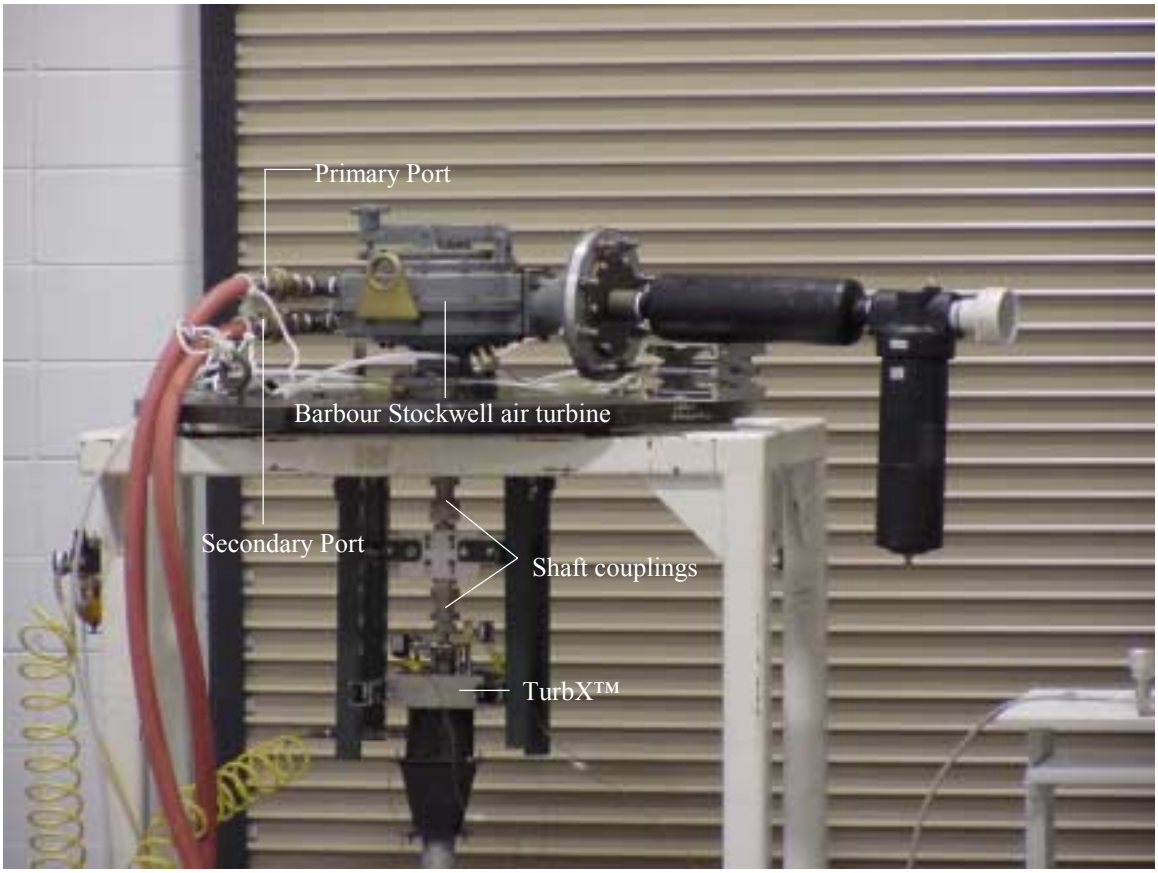

Figure 10. Barbour Stockwell air turbine and the TurbX™ engine

Air-driven Tests

Air-driven tests require compressed air to be supplied to the TurbX™ engine at two locations, the spark plug port and the air bearing. The air inlet ports along with the fuel injection holes were completely sealed to prevent room air from entering the engine. The air entering the spark plug port expands through the TurbX™ engine and exits through the exhaust ports to produce work.

A laminar air flow meter was installed in the exhaust pipe to measure the volumetric flow rate of air. The laminar air flow meter, CME Digital Flowmeter Model Number 40L-5-1200A, measures temperature, absolute pressure and differential pressure of the air stream as it flows through the meter. These values are used to determine the actual volumetric flow rate, which is digitally displayed on a standard output unit supplied by the vendor.

When air is supplied to both the spark plug port and to the air bearing, the laminar air flow meter measures the total volumetric airflow rate required to spin TurbX™ at a certain speed plus the air leakage from the air bearing. From the preliminary tests, it was determined that for all air-driven tests over a range of useable gap settings, a regulator air bearing gage pressure of 275.79 kPa was sufficient to lift the rotor off the stator in the vertical orientation to spin TurbX™ up to speeds of 10,000 rpm.

For air-driven testing, the compressed air fed into the spark plug port resulted in counter-clockwise rotation of the rotor and the output shaft of the TurbX™ engine (looking down on it). At the same time supplying air to the primary port of the air turbine provided resistance as it tried to rotate clockwise retarding the motion of TurbX™. The resultant torque was transmitted throughout the entire coupled vertical

shaft and measured by the torque meter. The results for the air-driven tests will be documented in more detail and presented in a thesis by Frederick Mottley.

Fired Tests

Upon completing the air-driven tests, the air inlet ports along with the fuel injection holes were completely unsealed and cleaned for the fired tests. A spark plug to ignite the air-fuel mixture was installed in TurbX™ and stainless steel fuel lines were connected to supply fuel from the compressed methane tank to the TurbX™ engine. A fully electronic, non-mechanical ignition system, MSD Blaster Ignition Model Number 5900, along with a pulse generator was used to create a spark. The original pulse generator setting was fixed at 50 sparks/second with an approximate duration of 0.002 seconds.

A glow plug was installed in place of the spark plug to ignite the air-fuel mixture because the spark plug did not ignite the air-fuel mixture at the original pulse generator setting. Once electrical power to the glow plug was turned on, the head of the plug would heat up within a few seconds and turned cherry red in color. As the temperature increased, the head of the plug would thermally expand and make contact with the rotor causing the rotor to decrease in rotational speed. Unless power was turned off, the rotor would eventually stop because the tip of the glow plug would interfere with the rotor. With the glow plug on, combustion was never initiated. The constant rotation of the rotor induced circulating airflow blowing past the head of the plug cooling it down and never allowing the glow plug to reach hot enough temperatures to ignite the air-fuel mixture. Because of these problems and limited time available, retracting the glow plug was not an

option; therefore it was removed and replaced with the spark plug. For the runs reported in this study the spark pulse generator was set to a larger value of approximately 100 sparks/second.

For the fired tests, the Barbour Stockwell air turbine was used as both a dynamometer and a starting device for TurbX™. To start the TurbX™ engine, air was supplied to the secondary port of the air turbine to initially spin TurbX™ in the counter-clockwise direction. The power to the spark plug signal generator was turned on and fuel was injected into TurbX™ at any time thereafter. Once the fuel supply was turned on, the TurbX™ engine should have become self-sustaining and therefore the air supplied to the secondary port of the Barbour Stockwell air turbine could be turned off.

Compressed technical grade methane (98% CH_4) was used as the fuel in the fired tests. The fuel flow rate was measured by a Tylan FM-360 series Mass Flow Meter capable of measuring flow rates up to 20 slpm. For safety reasons the fuel flow rate is controlled by a pneumatic-actuator bellow-sealed valve, Swagelok Part Number SS-4BK-1C, which is normally in the closed position and can be opened by pressurized air. The compressed air supply was used to actuate the bellow to let fuel flow from the compressed methane tank to the TurbX™ engine. Compressed air from the same source was also used to run the Barbour Stockwell air turbine. Should the compressor ever fail with the TurbX™ engine running in the firing mode, the pneumatic valve automatically cuts off, to prevent a potentially dangerous accumulation of gaseous fuel in the testing laboratory. A schematic of the fired tests fuel flow control system and instrumentation is shown in Figure 11.

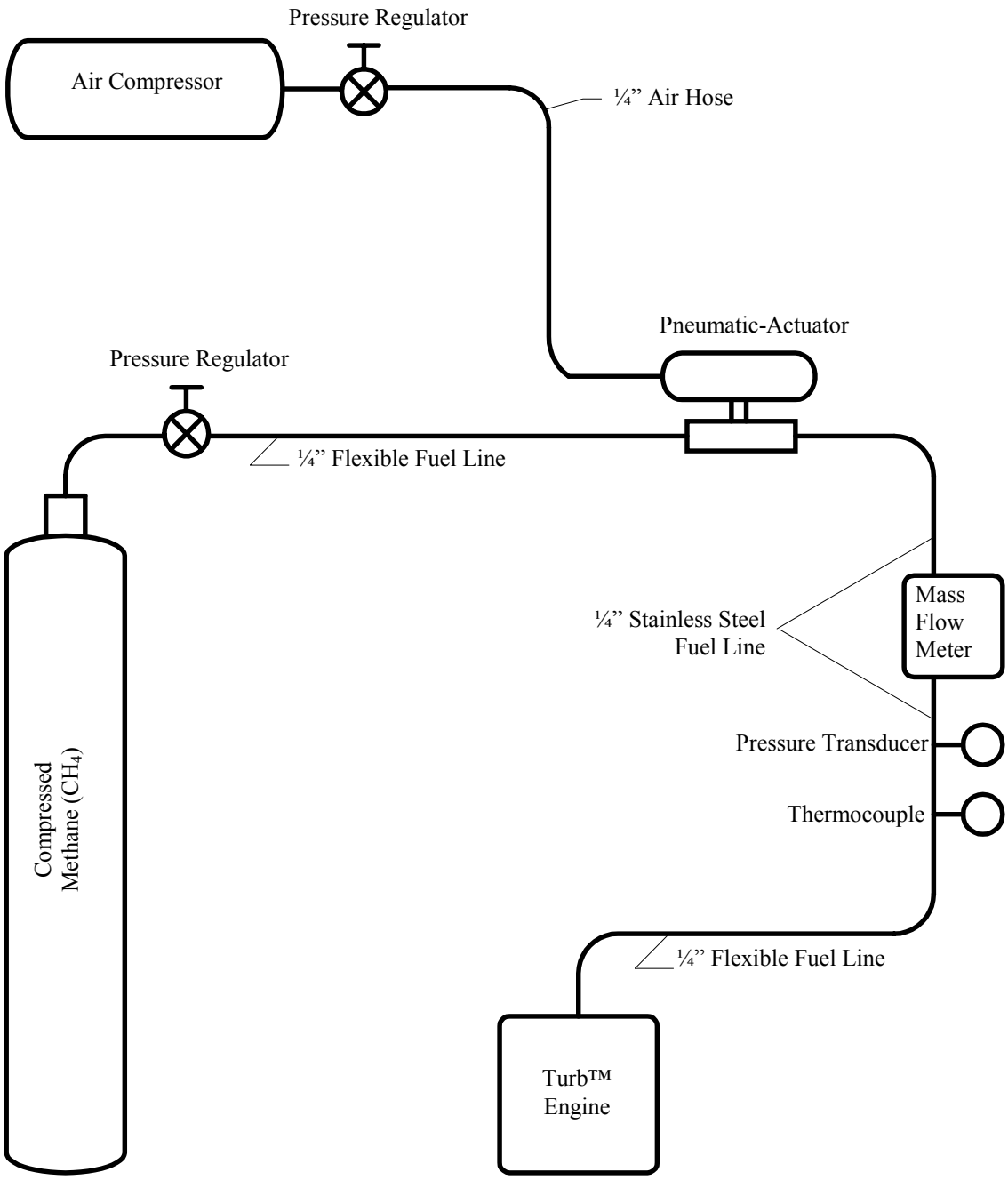

Figure 11. Schematic showing fired tests fuel flow control system and instrumentation

The laminar air flow meter was not used in the exhaust pipe during fired tests because its maximum temperature limit would have been exceeded. The inlet airflow rate could not be measured by the laminar air flow meter because of geometric complexities associated with the arrangement of the air inlet ports on the TurbX™ engine. It is important to note that, by design, a certain unknown portion of the entering air blows exhaust products away from the rotor and out through the exhaust ports. Even if it were possible to measure the volumetric airflow rate entering the engine, it would not be possible to determine the actual flow rate of air entering the combustion stage.

For the fired tests, pressure and thermocouple temperature sensors were installed in the combustion chamber and the last stator expansion passage. The stator that contains the spark plug had no available space to install the pressure and temperature sensors in the combustion chamber. Therefore, the pressure and temperature sensors were located in the combustion chamber across from the rotor on the opposite side of the stator containing the spark plug. The pressure sensor (P_{gc}) measured gas gage pressure inside the combustion chamber and the temperature sensor (T_{gc}) measured gas temperature inside the combustion chamber. The temperature sensor (T_{ge}) measured the gas temperature of the last stator expansion passage. An additional temperature sensor (T_{wc}) measured the wall temperature of the combustion chamber located in the same combustion chamber as the other sensors. The wall temperature thermocouple was located on a thin section of metal at the farthest down stream location of the combustion chamber and very close to the rotor. This region was later found to have hot spots evidenced by the metal discoloration.

A Note About Project Deadline and Delays Associated with Engine Failures

The deadline to complete this project was September 30, 2001 and the test bay had to be cleared of all hardware associated with this project at the end of the day. The safety procedures approved by ORNL were followed throughout during the conduct of all the tests reported in this thesis.

During the air-driven tests, on August 17 and 21 the engine seized due to rotor - stator galling. In each instance, the stators and rotor were repaired and the testing was resumed. The air-driven tests were completed on August 21, 2001. During the next four weeks the test rig was modified for fired tests and passed a safety inspection. The rig was ready on September 19, 2001.

The first fueled or fired test was conducted on September 20, 2001. The engine ran well for about 40 minutes at a speed of 5188 rpm and then the rotor froze. When the engine was disconnected from the test stand and disassembled, two problems were observed. The first observation was that the welded inconel pieces (weldment) across the second and third stator expansion passages of the top stator were missing. They were found in the air-bearing space in the bottom stator. It should be pointed out that the stator passages were originally created by carving out material to create a U-shaped groove and then welding an insert across the top. The resultant space between the weldment and the U-shaped groove served as the expansion passage. The second observation was that dark purple hot spots were found on the top stator just downstream of the combustion chamber and the rotor was free of hot spots. From these two observations, it can be concluded that the stator might have reached temperatures high enough to weaken the weldments resulting in their subsequent failure, and that the rotor remained cool relative to the

stators. The inconel pieces were welded back on to the stator, the stator surface was refinished and the testing was resumed on September 26, 2001. During the next two days of testing, there was no significant temperature rise associated with combustion for high speeds. On September 28, 2001 the spark plug was replaced with a glow plug to help combustion at the higher speeds. During the ensuing testing no improvement in combustion performance was observed. The problems associated with the thermal expansion of the glow plug are discussed above in this chapter. The spark plug was reinstalled and the testing was resumed on September 29, 2001. For all the reasons cited above, useful tests could only be performed on the last day, September 29, 2001, of this project.

CHAPTER 5
RESULTS AND DISCUSSION

The fired tests were performed during the day of September 29, 2001. The tests were conducted on this day only because of time limitations. A total of 26-fired tests were conducted to measure the TurbX™ engine performance characteristics as a function of speed. The Barbour Stockwell air turbine was used to start the TurbX™ engine during the 26-fired tests. The airflow rate supplied to the Barbour Stockwell air turbine remained constant throughout each individual test run, which allowed TurbX™ to spin at a constant set speed. The compressed air supplied to the Barbour Stockwell air turbine was limited by the excessive pressure drop in the air hose, which restricted TurbX™ from being tested at its design speed of 20,000 rpm. The prototype TurbX™ engine had no cooling system and this limited fuel injection duration in each test run to a range between 60 and 360 seconds to prevent the engine from overheating. It should also be pointed out that the suction pressure created by the fan blades, located on the outer perimeter of the rotor, draw in atmospheric air. The exhaust gases leave the engine at atmospheric pressure as well. Unlike the Brayton cycle where a compressor supplies pressurized air to the combustion chamber, the air in the prototype TurbX™ engine is at nearly atmospheric pressure as it reaches the combustion chamber. In this sense, it can be said that for the tests conducted in this study, the pressure ratio is one prior to combustion.

The data obtained from all 26-test runs were plotted on identical horizontal and vertical scales to make it easier to compare the results of the different runs. Measured fuel flow rate, gage pressure inside the combustion chamber ($P_{gc} - P_a$), output torque,

wall temperature inside the combustion chamber (T_{wc}), gas temperature inside the combustion chamber (T_{gc}) and gas temperature of the last stator expansion chamber (T_{ge}) are plotted as a function of time.

The size of the air original gap setting for the first set of test runs is approximated to be 0.000018 m (0.0007 in) on each side of the rotor. At this position the original gap is considered to be *zero turns*. The gap size was decreased a total of three times after the initial setting resulting in a gap change on each side of the rotor of approximately 0.000013 m (0.0005 in). The first, second and third gap changes are labeled *one turn*, *two turns* and *three turns*, respectively. The maximum gage pressure measured inside the combustion chamber ranged from approximately 3 to 15 kPa. The air bearing appeared to function reasonably well in that it allowed the rotor to rotate nearly frictionless.

In some test runs, the plots illustrate the measured values of the gas temperature inside the combustion chamber (T_{gc}), increased rapidly to a value of 500°C and appeared to stay at that value while the measured wall temperature inside the combustion chamber (T_{wc}), also increased but trailed behind T_{gc}. However, once the T_{wc} thermocouple indicated a temperature of approximately 400°C, the fuel was turned off and the TurbX™ engine was air cooled down by its own fan to approximately 100°C before the start of the next run. It should be pointed out that T_{gc} does not exceed 500°C because the range of the input modules for all three thermocouples was limited to 0 to 500°C. Although the gas temperature might have exceeded 500°C, it was not detected because of the limit of the thermocouple input module. In this study combustion is considered to be satisfactory, whenever the temperature of the gases inside the combustion chamber (T_{gc}) reached values in excess of 500°C and the trailing wall temperature inside the combustion

chamber (T_{wc}) also increased to values of 400°C or greater. On the other hand combustion is considered to be unsatisfactory, whenever either one or both of the temperature sensors inside the combustion chamber measured values well below 400°C.

The TurbX™ engine was tested at selected rotational speeds ranging from 1818 to 9590 rpm. All 26 fired test runs were categorized into three separate cases based on rotational speed and the general quality or nature of combustion: Case A, low rotational speeds ranging from 1818 to 4028 rpm; Case B, medium rotational speeds ranging from 4690 to 7520 rpm; Case C, high rotational speeds ranging from 8200 to 9590 rpm. At any given rotational speed the air swept in by the TurbX™ engine remained practically constant. In each of the 26 constant speed tests, fuel flow rate supplied to TurbX™ was slowly increased and therefore the fuel-air ratios were increased from zero to a stoichiometric value. Fuel flow rates in excess of stoichiometric values were not used in the present tests.

Case A is categorized according to low rotational speeds ranging from 1818 to 4028 rpm. The plots for this case are shown in Figures 12 through 15. Figure 12 illustrates that during the majority of the fuel injection time interval, the measured wall temperature inside the combustion chamber (T_{wc}) is greater than the measured temperature of the gases inside the combustion chamber (T_{gc}). This unexpected temperature behavior can be explained in terms of the ratio of rotor to flame velocity. The rotor velocity is significantly higher than the laminar and even turbulent flame velocities as indicated and explained in Appendix A. Before the combustion gases reach the thermocouple T_{gc} located on the opposite stator, because of its higher velocity, the rotor tends to sweep the burning gases in the direction toward the region where T_{wc}

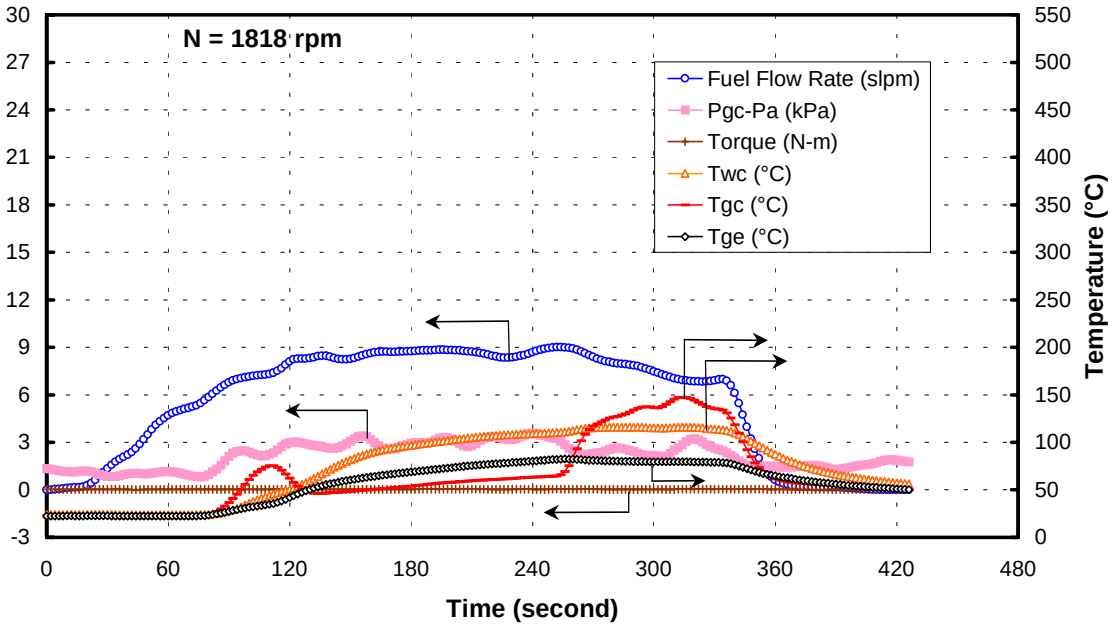

Figure 12. Case A, N = 1818, zero turns in from original gap setting

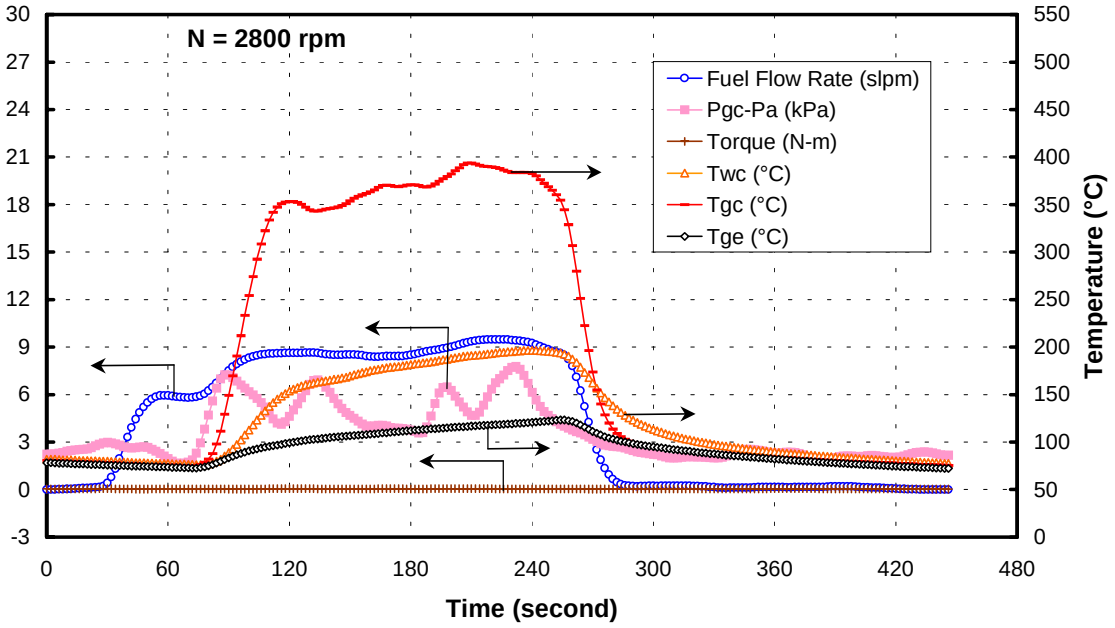

Figure 13. Case A, N = 2800, three turns in from original gap setting

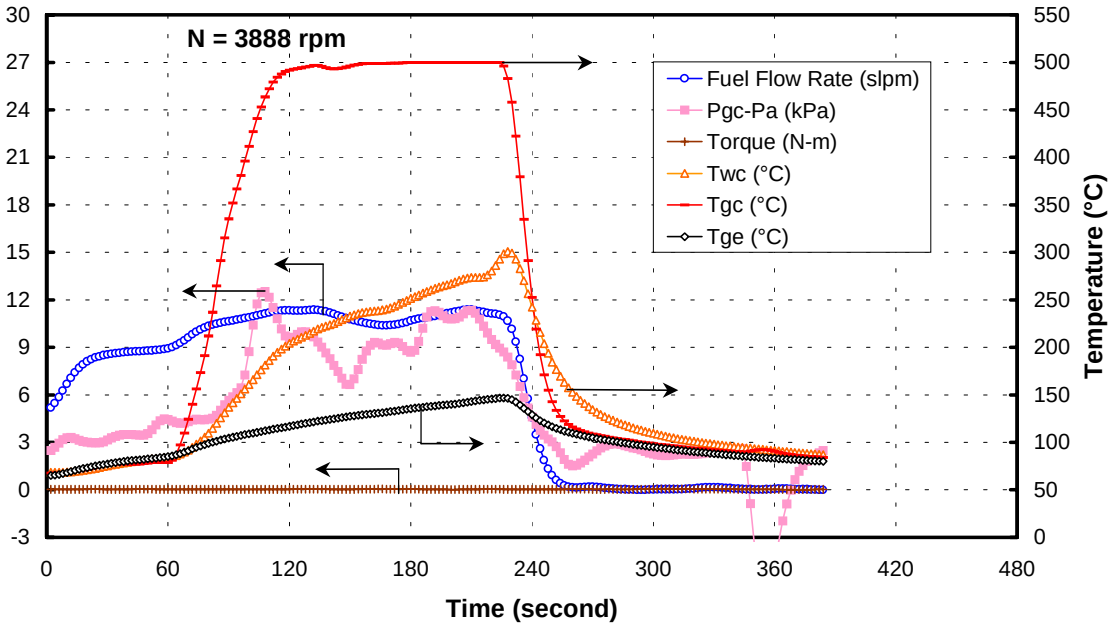

Figure 14. Case A, N = 3888, three turns in from original gap setting

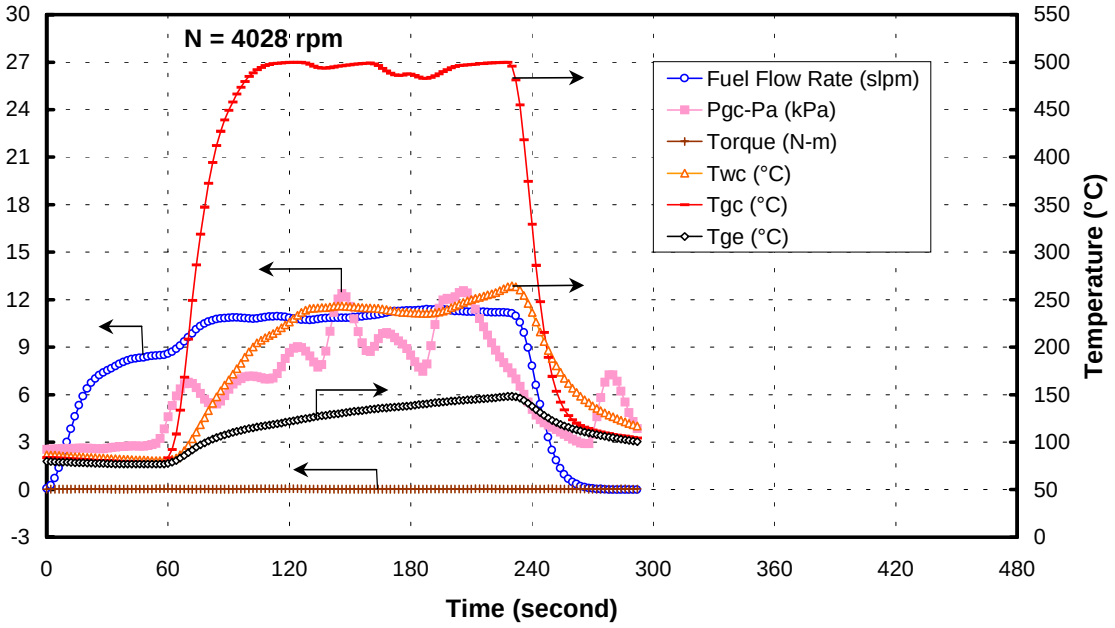

Figure 15. Case A, N = 4028, three turns in from original gap setting

thermocouple is located resulting in $T_{wc} > T_{gc}$. Both temperature sensors inside the combustion chamber measured values well below 400°C, indicating unsatisfactory combustion. When there was satisfactory combustion, as most runs in Case B to be discussed next, the temperature distributions tend to be more normal where gas temperature T_{gc} leads the wall temperature T_{wc}. In Figures 13 through 15, T_{gc} is significantly greater than T_{wc}. The T_{wc} thermocouple sensor measured values well below 400°C, indicating unsatisfactory combustion.

The maximum gage pressure measured inside the combustion chamber for Case A ranged from approximately 3 to 13 kPa. The air-bearing gap seemed to have an effect on pressure rise given that maximum gage pressure is greater for Figures 13 through 15 with a gap setting of three relative to Figure 12 with a gap setting of zero. However, regardless of the gap setting the measured gage pressure inside the combustion chamber was not sufficient for TurbX™ to develop torque. The results of Case A clearly indicate TurbX™ produced no net positive torque and therefore no power was generated.

Case B is categorized according to medium rotational speeds ranging from 4690 to 7520 rpm. The plots for this case are shown in Figures 16 through 33. All runs in Case B illustrate that during the short fuel injection time interval the temperature of the gases inside the combustion chamber (T_{gc}) reached values of 500°C and the wall temperature inside the combustion chamber (T_{wc}), also increased but trailed slightly behind T_{gc}. Once T_{wc} reached a value beyond approximately 400°C fuel flow rate supplied to TurbX™ was slowly turned off. The fact that for all runs in Case B both T_{gc} reached 500°C and T_{wc} reached approximately 400°C indicated that satisfactory combustion was achieved.

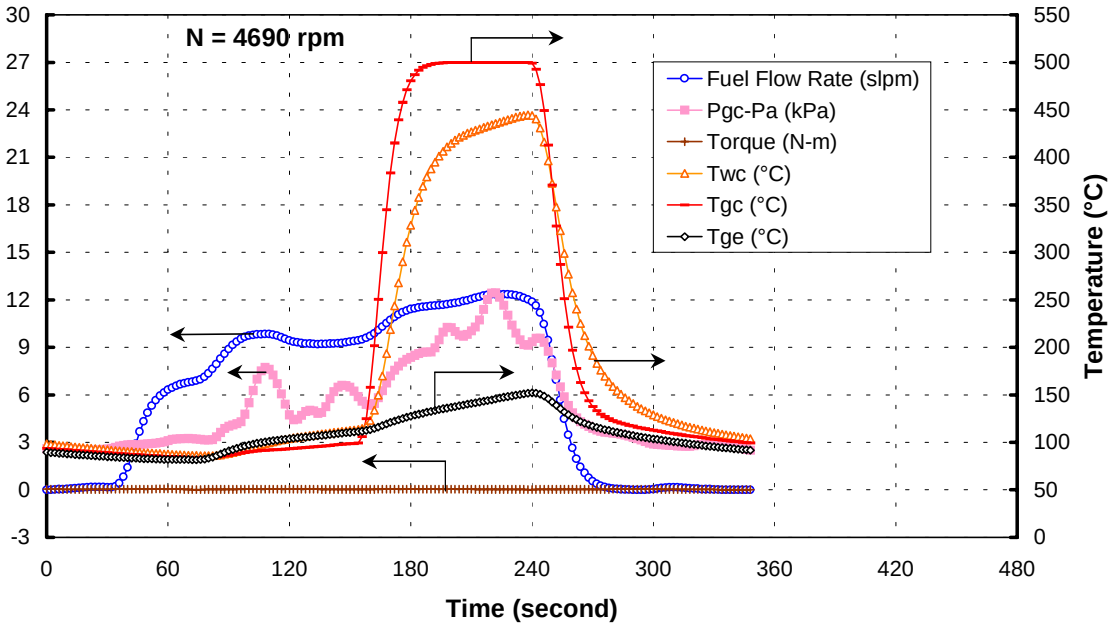

Figure 16. Case B, N = 4690, three turns in from original gap setting

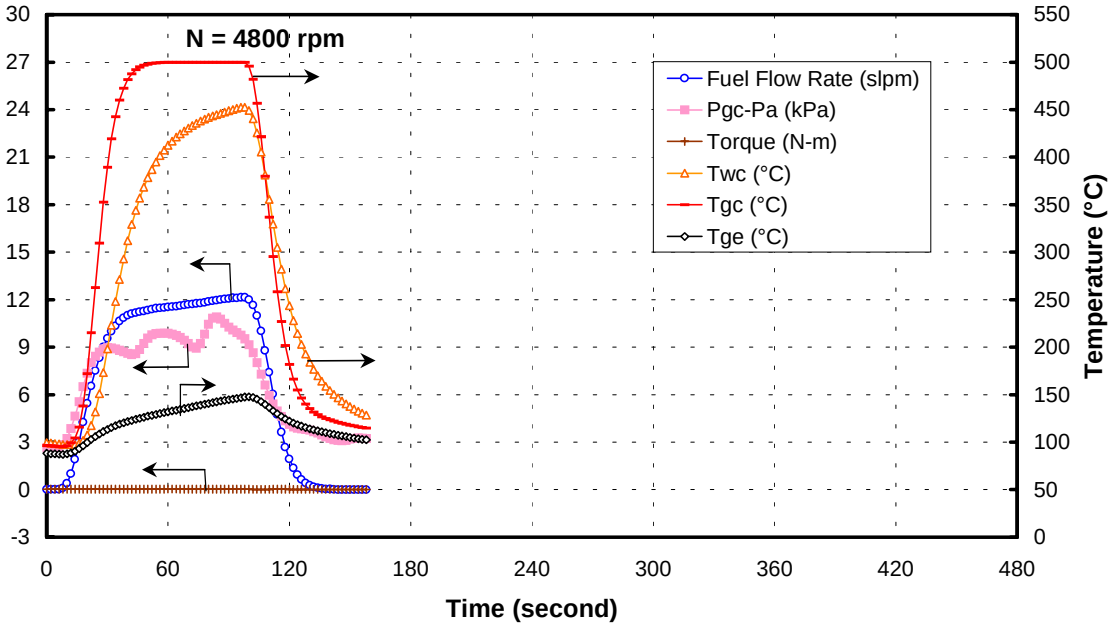

Figure 17. Case B, N = 4800, three turns in from original gap setting

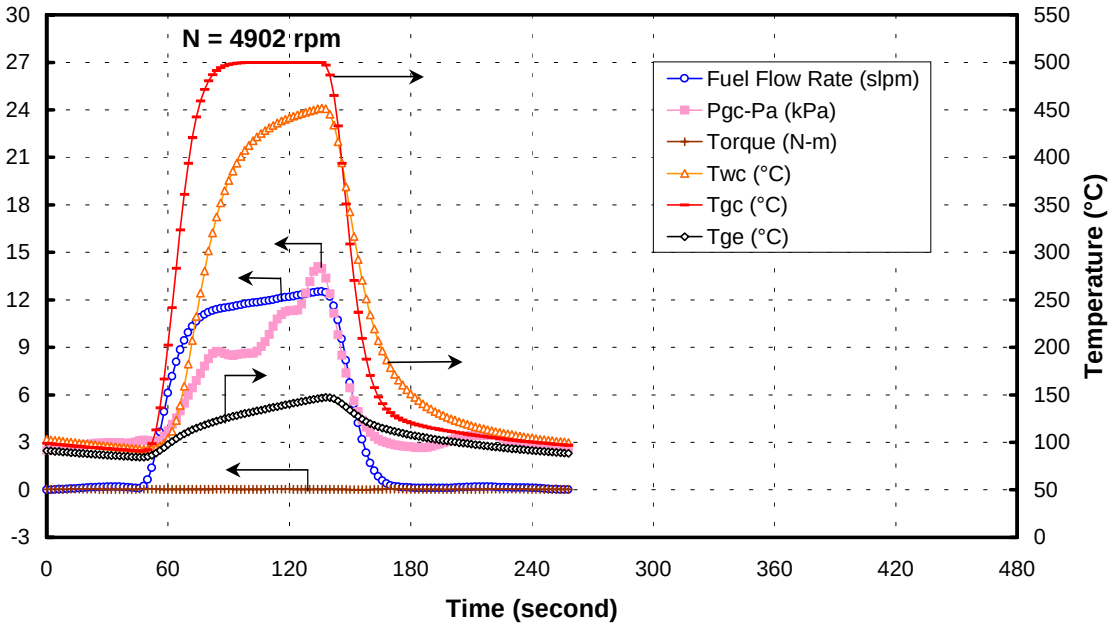

Figure 18. Case B, N = 4902, three turns in from original gap setting

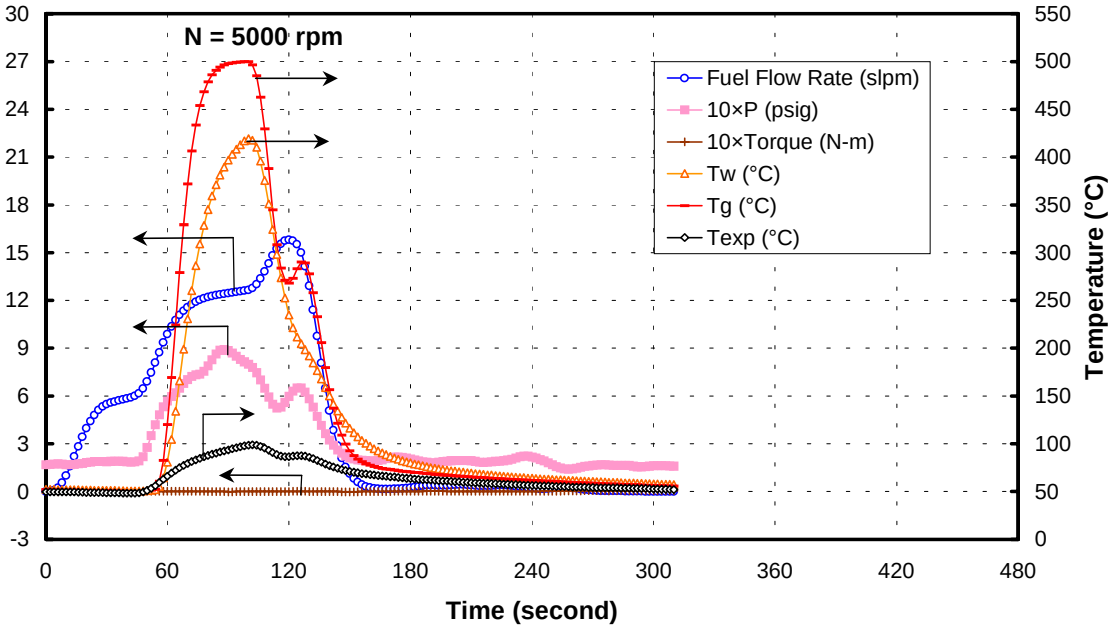

Figure 19. Case B, N = 5000, zero turns in from original gap setting

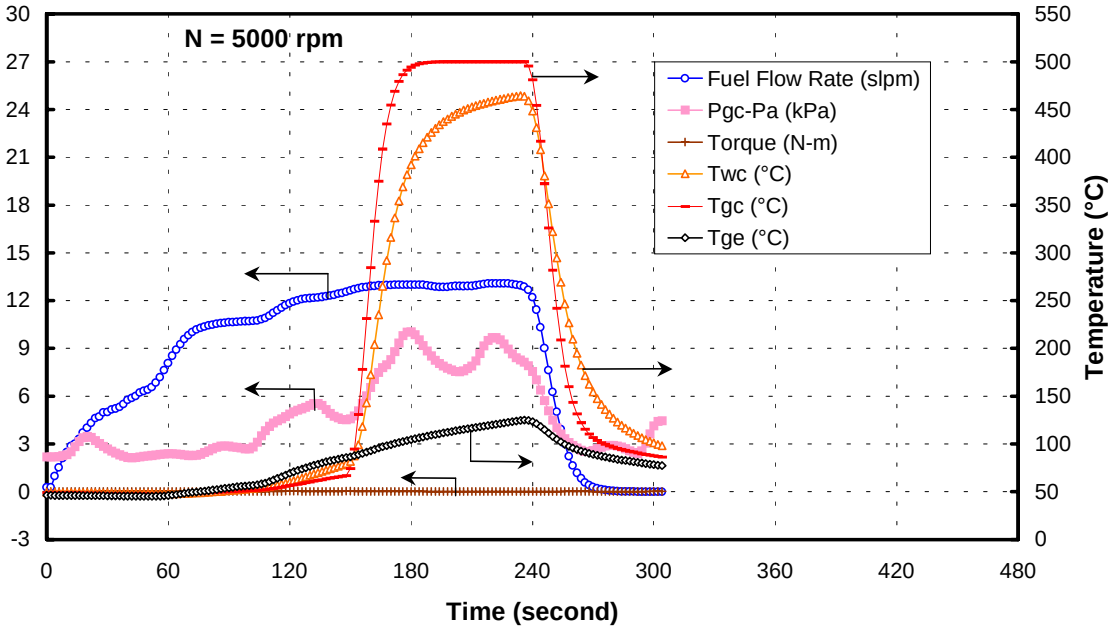

Figure 20. Case B, N = 5000, two turns in from original gap setting

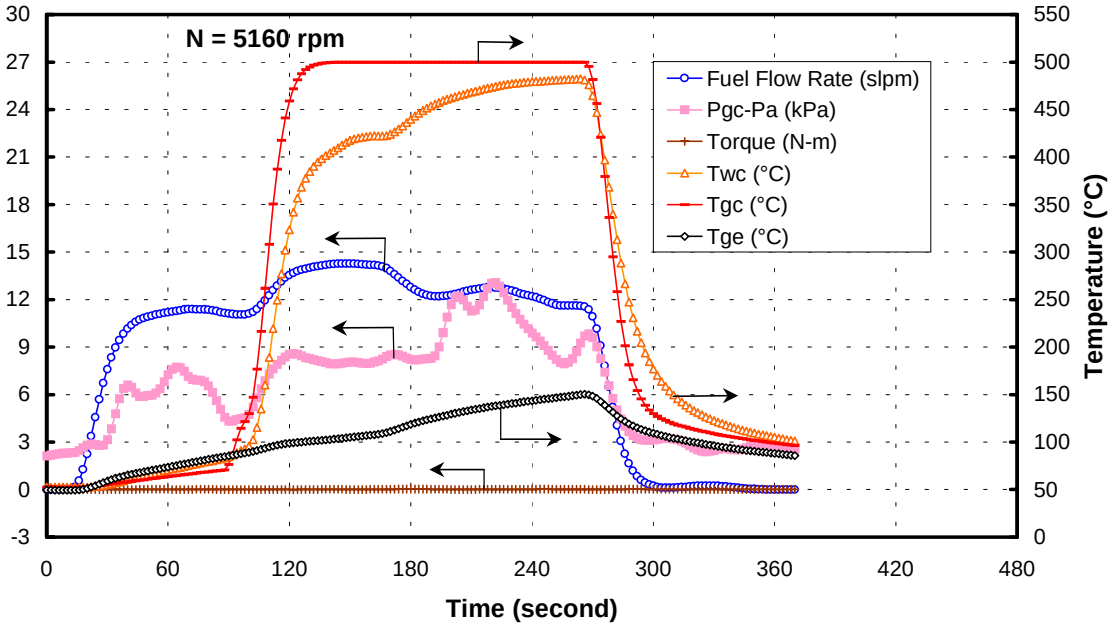

Figure 21. Case B, N = 5160, three turns in from original gap setting

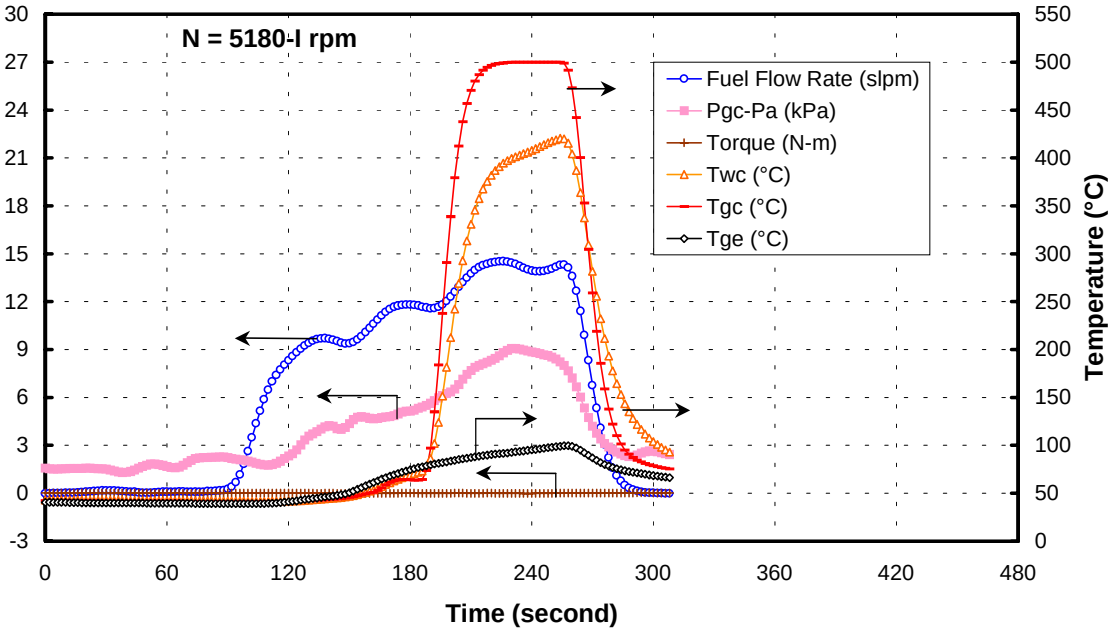

Figure 22. Case B, N = 5180-I, one turn in from original gap setting

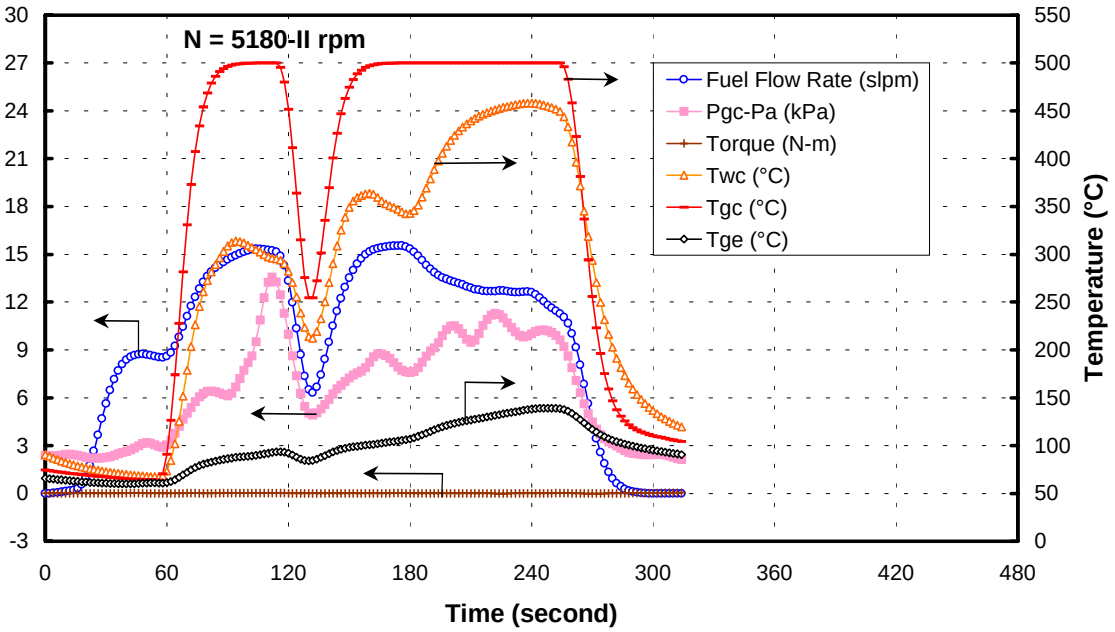

Figure 23. Case B, N = 5180-II, one turn in from original gap setting

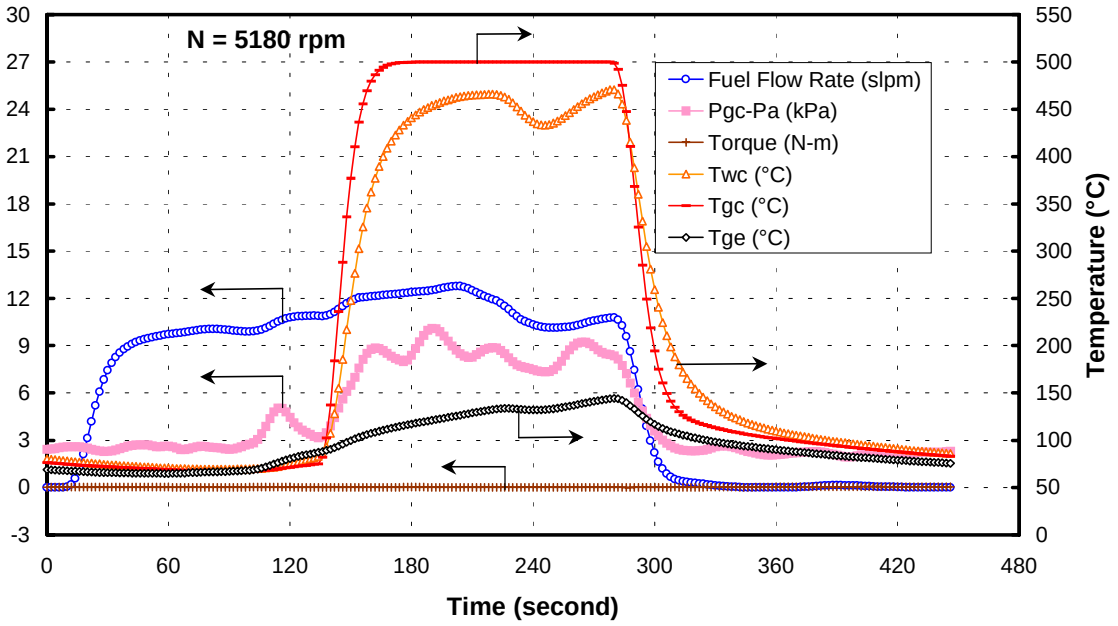

Figure 24. Case B, N = 5180, two turns in from original gap setting

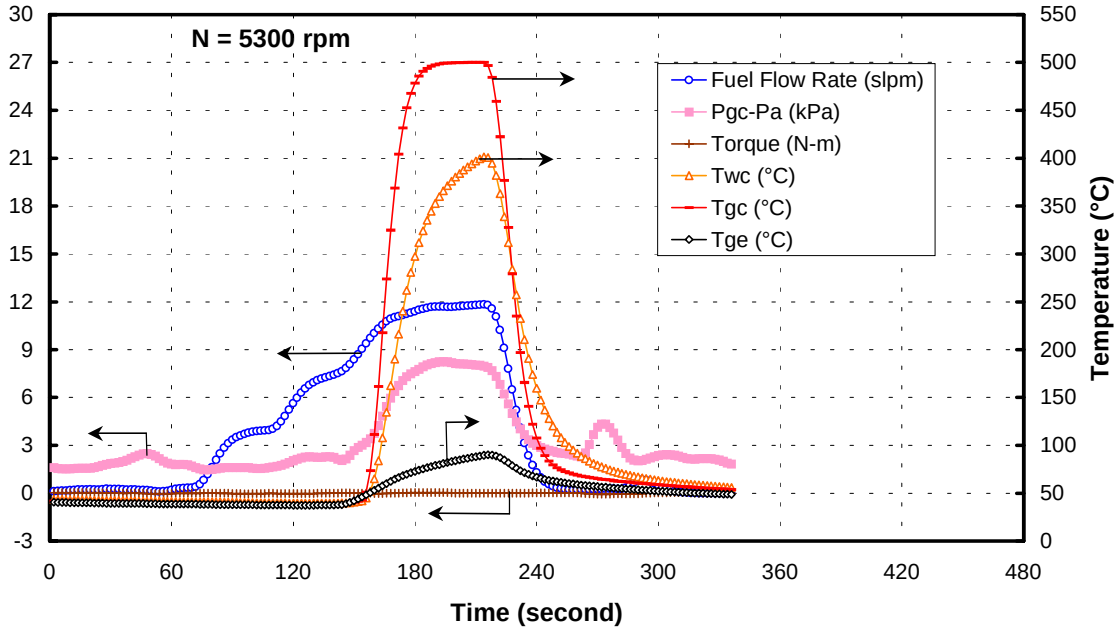

Figure 25. Case B, N = 5300, zero turns in from original gap setting

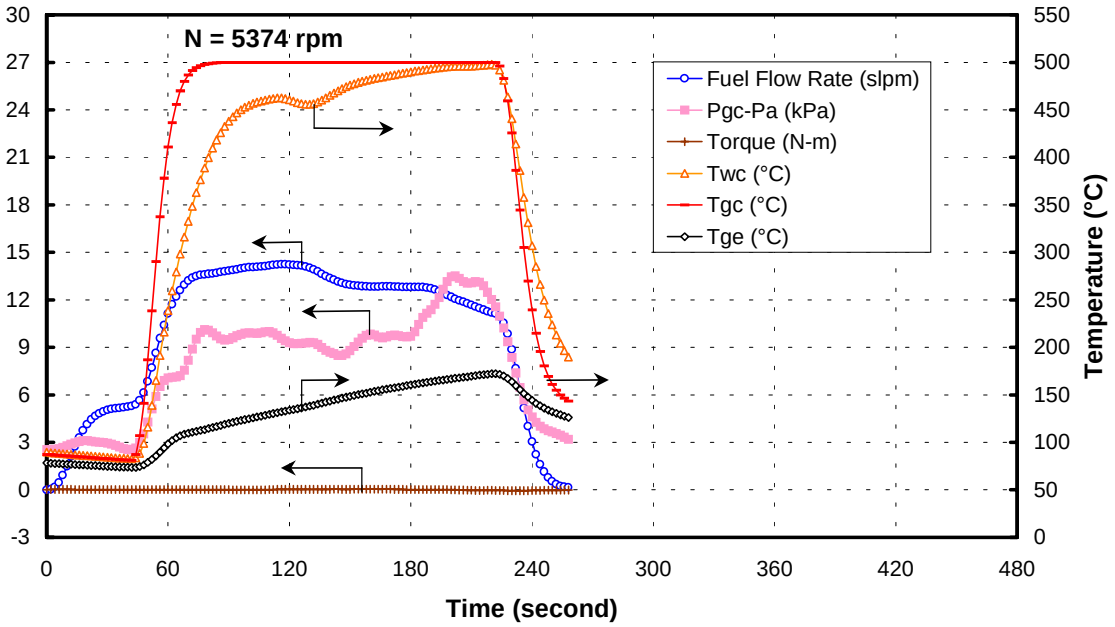

Figure 26. Case B, N = 5374, three turns in from original gap setting

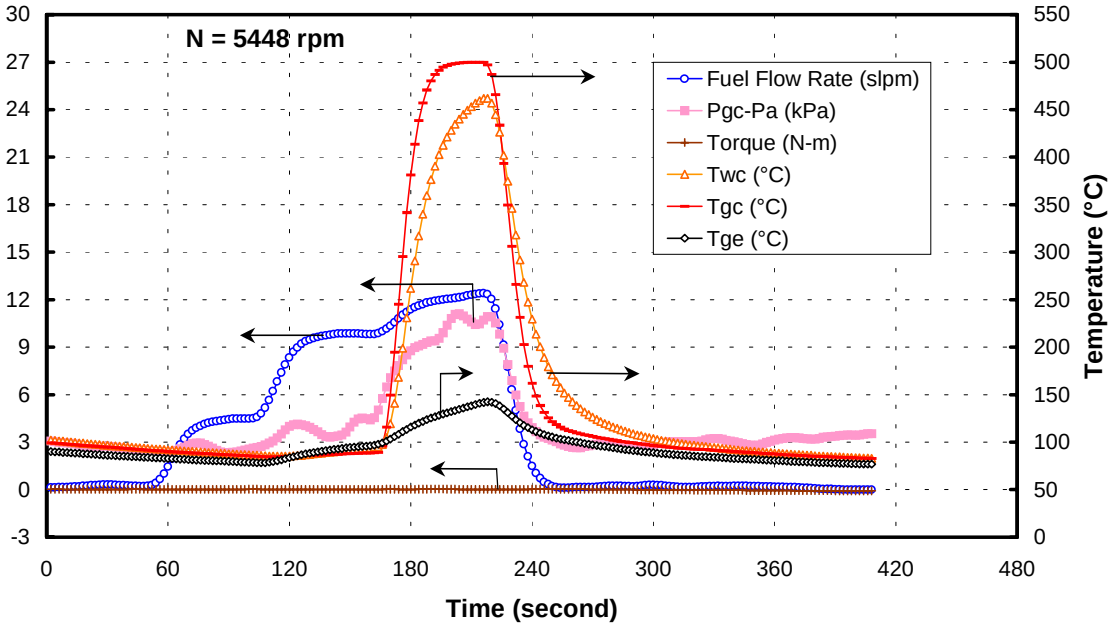

Figure 27. Case B, N = 5448, three turns in from original gap setting

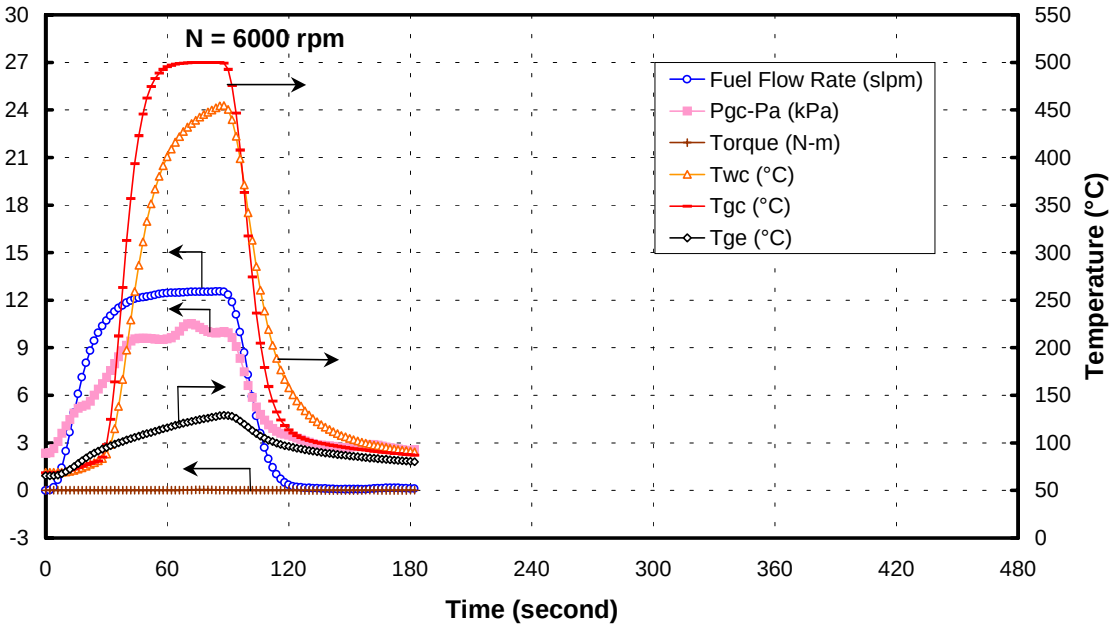

Figure 28. Case B, N = 6000, three turns in from original gap setting

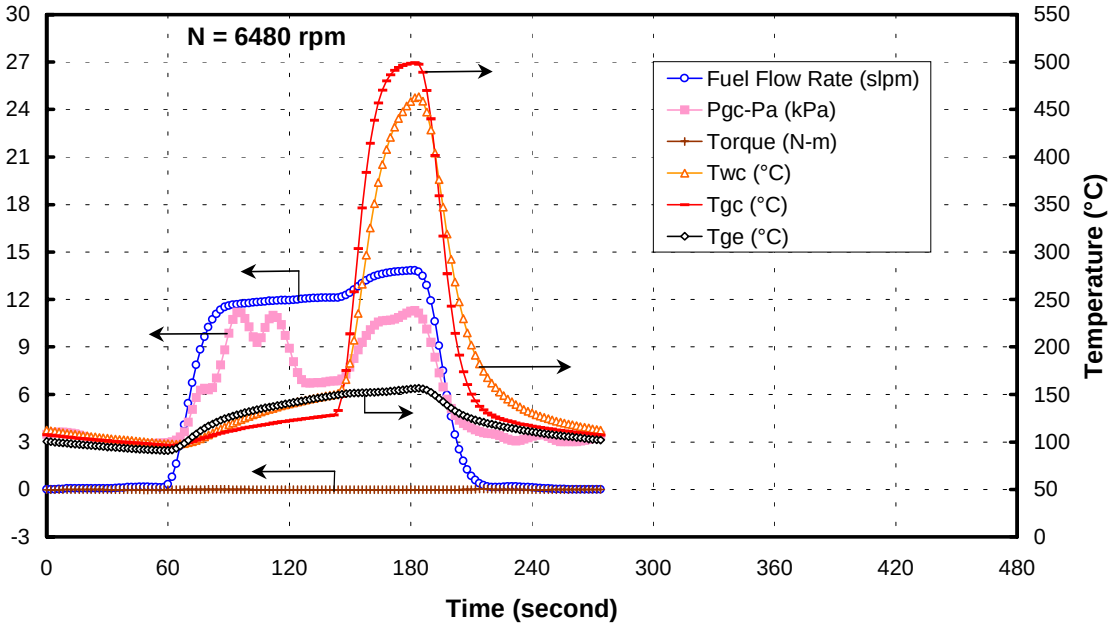

Figure 29. Case B, N = 6480, three turns in from original gap setting

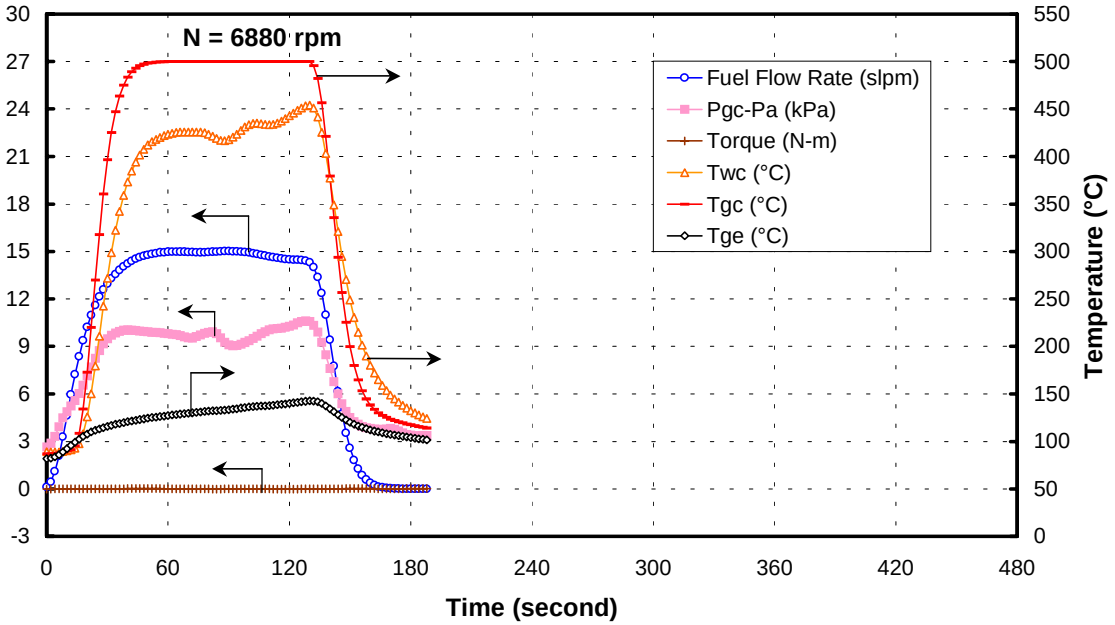

Figure 30. Case B**,** N = 6880, three turns in from original gap setting

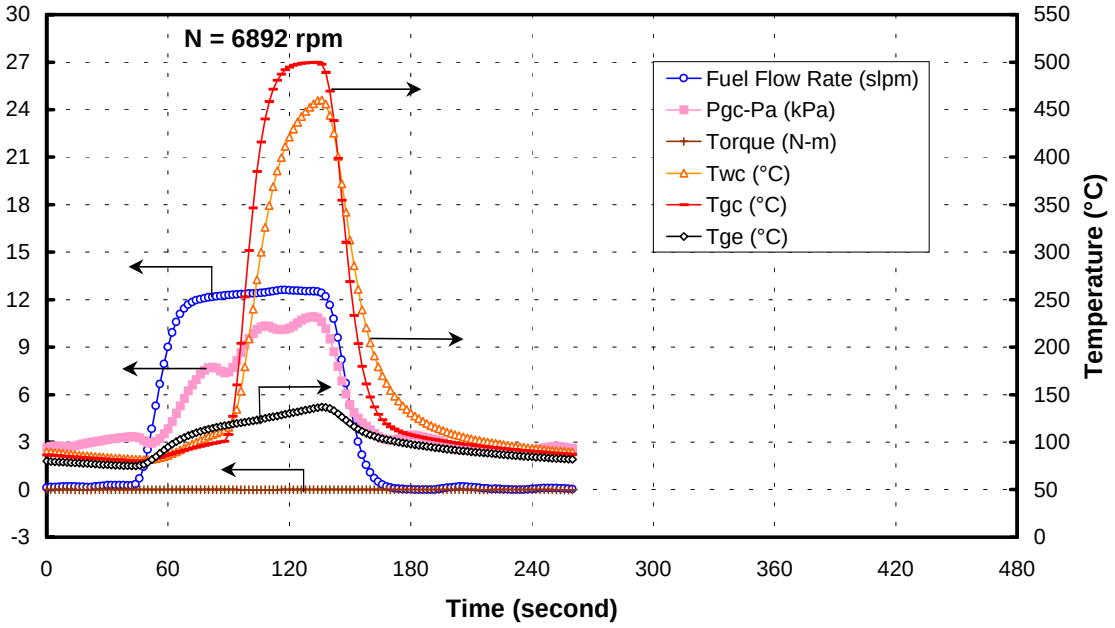

Figure 31. Case B, N = 6892, three turns in from original gap setting

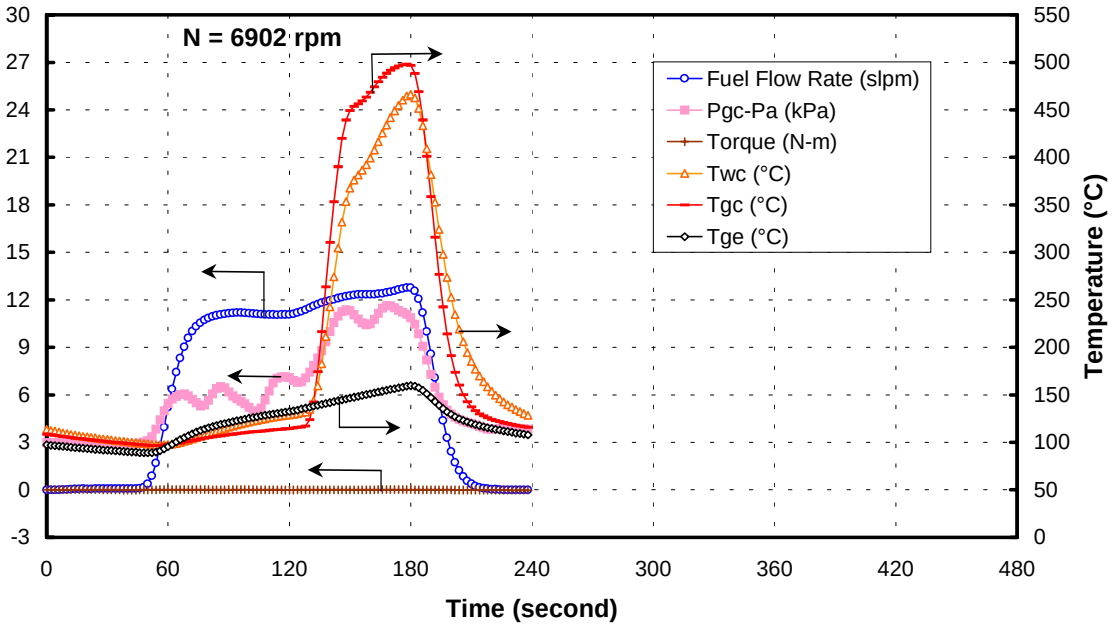

Figure 32. Case B, N = 6902, three turns in from original gap setting

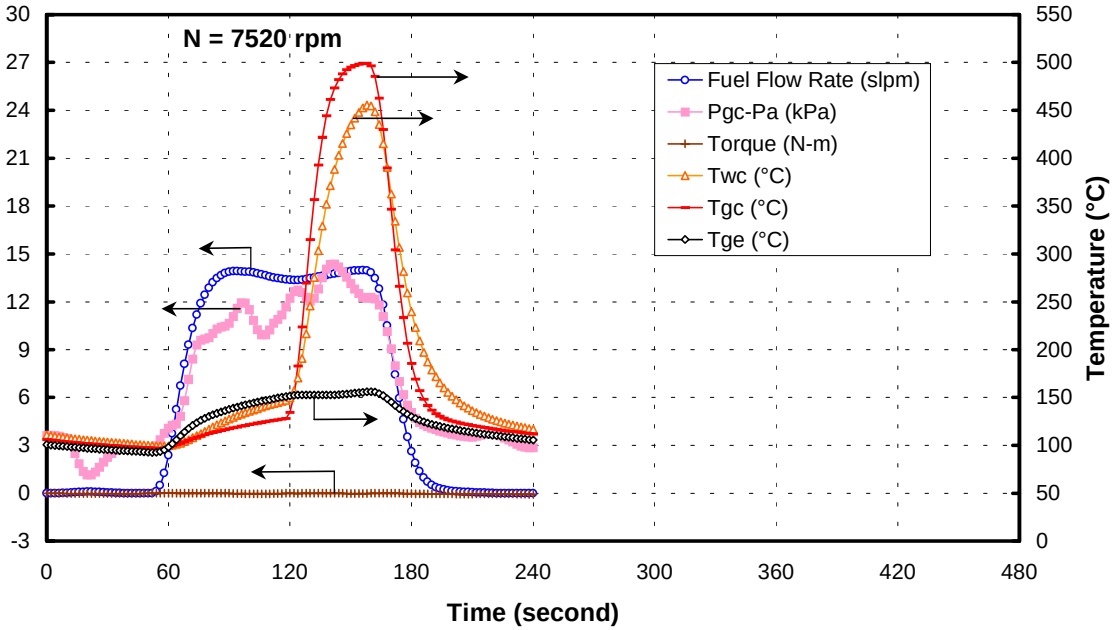

Figure 33. Case B, N = 7520, three turns in from original gap setting

For the test runs at 6480, 6902 and 7520 rpm shown in Figures 29, 32 and 33, it can be seen that (1) during the first 30-seconds to one-minute of fuel injection the maximum temperatures inside the combustion chamber were under about 150°C indicating unsatisfactory combustion, and (2) during this period the gas temperature in the last expansion stator passage (T_{ge}) is found to have exceeded the gas temperature inside the combustion chamber (T_{gc}). An explanation for this temperature abnormality is provided in Appendix B. After this period of time, as fuel flow rate increased, T_{gc} increased rapidly to values in excess of 500°C indicating satisfactory combustion.

The above results indicate that the rate of increase of fuel flow rate is a factor. When the fuel flow rate is increased rapidly, satisfactory combustion was observed without the temperature abnormalities. On the other hand, combustion tends to be unsatisfactory when fuel flow rate increase is not as rapid during the first 30 to 60 seconds of fuel injection. Even in this situation, further increases in fuel flow rate ultimately resulted in satisfactory combustion as indicated by the high temperatures observed.

The maximum gage pressure measured inside the combustion chamber for all runs in Case B ranged from approximately 8 to 14 kPa. The air-bearing gap seemed to have an effect on pressure rise in the combustion chamber in runs with medium rotational speeds. When the air-bearing gap was set at the initial setting of zero turns the maximum gage pressure reached values of approximately 8 and 9 kPa. Decreasing the gap setting by one turn resulted in maximum gage pressure values of approximately 9 and 13 kPa. Runs with a gap setting of two turns resulted in maximum gage pressure values of approximately 10 kPa and in general, the runs with a gap setting of three turns

indicated greater gage pressure rises ranging from approximately 10 to 14 kPa. The gap setting seemed to have an impact on the pressure rise in the combustion chamber. However, in spite of the satisfactory combustion observed in all runs in Case B, the maximum gage pressure measured inside the combustion chamber was not sufficiently high enough for TurbX™ to develop output torque and power.

Case C is categorized according to high rotational speeds ranging from 8200 to 9590 rpm. The plots for this case are shown in Figures 34 through 37. Figure 34 and Figure 37 illustrates that during the entire fuel injection time interval both the wall temperature inside the combustion chamber (T_{wc}) and the gas temperature of the last stator expansion chamber (T_{ge}) are greater than measured gas temperature inside the combustion chamber (T_{gc}). This unexpected temperature behavior can also be explained, as was done for some of the runs in Case A, in terms of the ratio of rotor to flame velocity. The details are discussed in Appendix A. Both temperature sensors inside the combustion chamber measured values well below 400°C indicating unsatisfactory combustion. On the other hand, Figure 35 and Figure 36 illustrates that T_{gc} reached a value of 500°C and T_{wc} reached 400°C or greater indicating that satisfactory combustion was achieved.

The maximum gage pressure measured inside the combustion chamber for Case C ranged from approximately 12 to 15 kPa. Since the air-bearing gap setting was not changed during these runs no conclusions can be drawn about the effect of the air gap setting and maximum gage pressure measured inside the combustion chamber. The results from Case C clearly indicate the TurbX™ engine did not produce any net positive torque and therefore no power was generated.

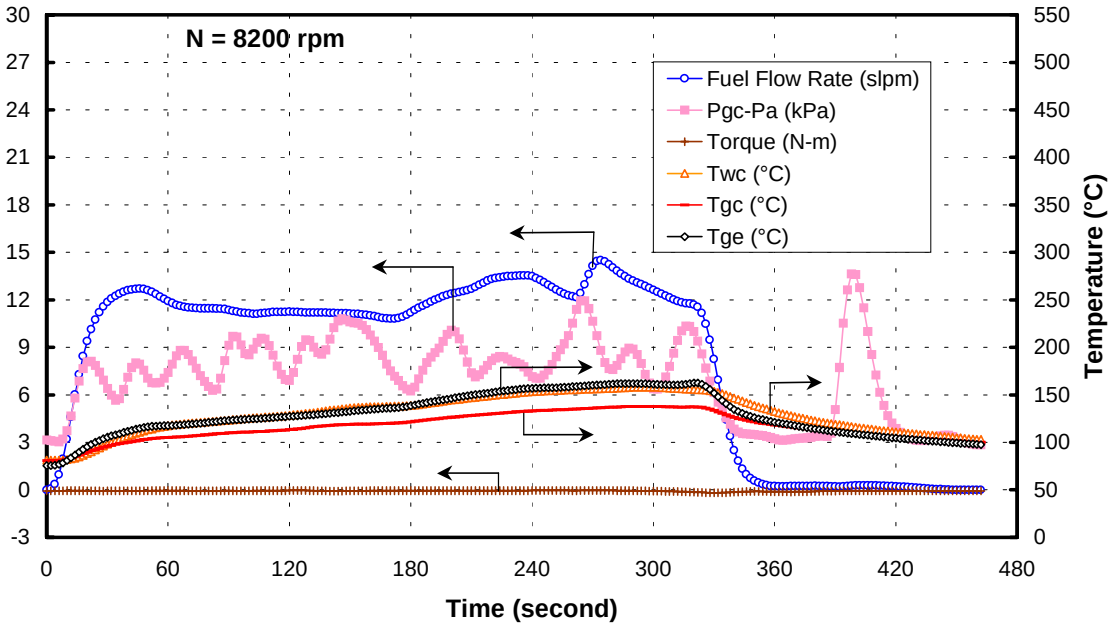

Figure 34. Case C, N = 8200, three turns in from original gap setting

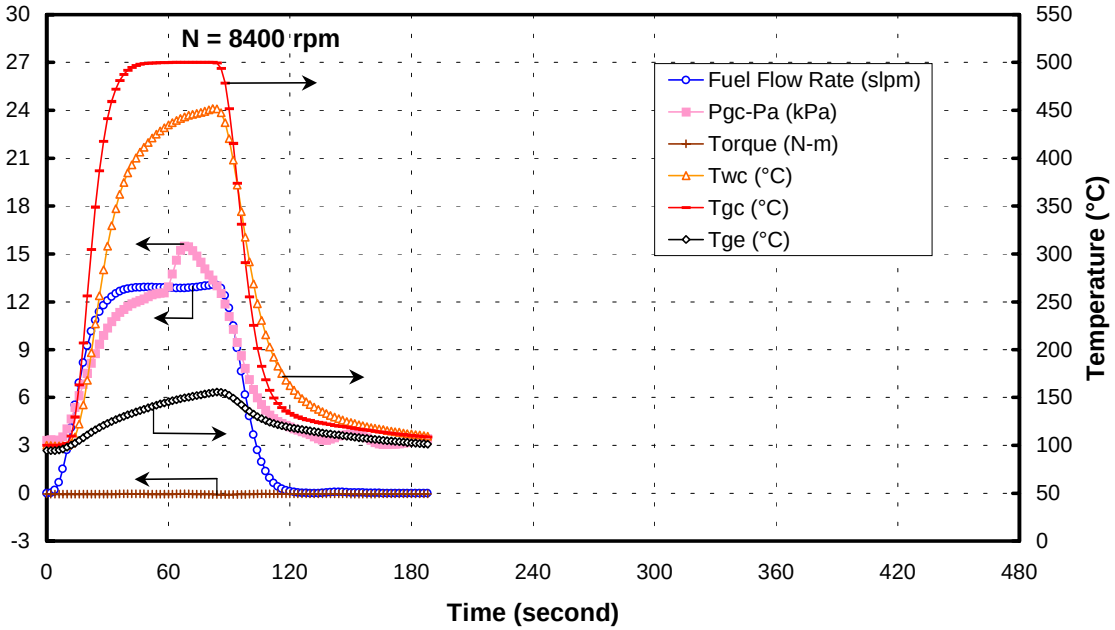

Figure 35. Case C, N = 8400, three turns in from original gap setting

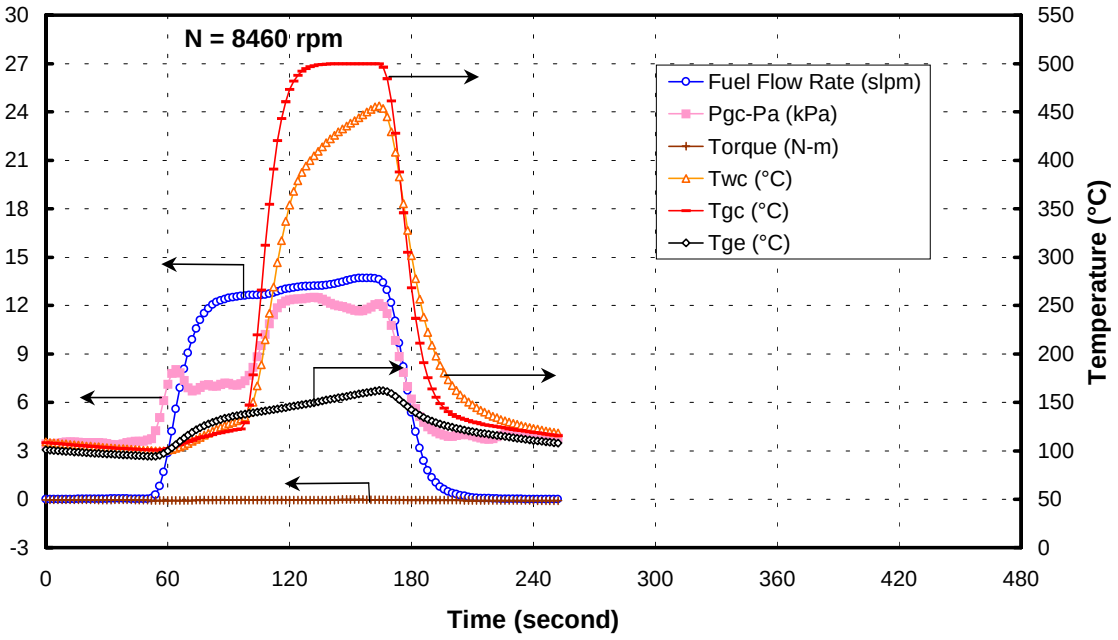

Figure 36. Case C, N = 8460, three turns in from original gap setting

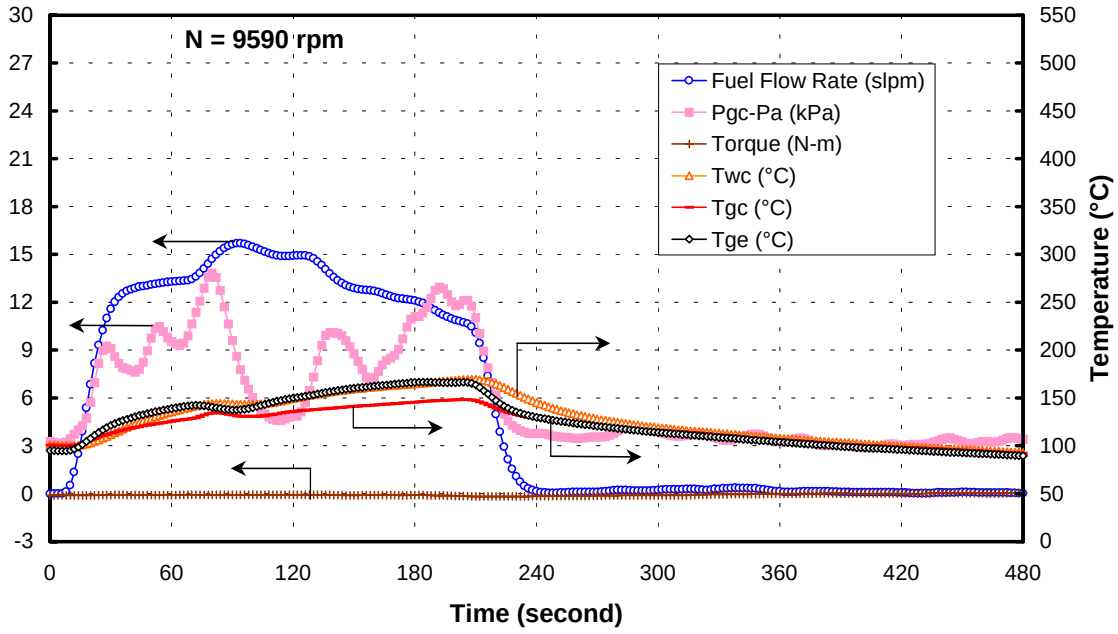

Figure 37. Case C, N = 9590, three turns in from original gap setting

Overall the results of all 26-fired tests indicate that the TurbX™ engine produced no net positive shaft torque and therefore no power was generated. Even in runs where combustion was satisfactory, the gage pressure inside the combustion chamber never exceeded 15.5 kPa. For this reason it was determined this prototype version of TurbX™ could not run without the help of the Barbour Stockwell air turbine. The low-pressure rise inside the combustion chamber is indicative of excessive leakage through the rotor/stator clearance gap in the bladed section of the air bearing.

Abbreviated summaries of the results for the constant speed fired tests are shown in Tables 1 and 2. In Table 1 peak combustion-chamber gage pressures were averaged according to the number of tests performed for each gap setting. The results indicate that decreasing the air gap, in general, increased the measured average gage peak pressure inside the combustion chamber. In Table 2 a summary for each of the test runs is presented. The test runs are broken down into three separate cases based on rotational speed and quality of combustion. In the last column the observed temperature contrasts are indicated.

Table 1. Effect of air-bearing gap setting on average of peak gage pressures in kPa

Air-bearing gap setting	In cases of satisfactory combustion	In cases of unsatisfactory combustion
Zero turns (max. air gap)	8.60	3.60
One turn	11.40	-
Two turns	10.10	-
Three turns (min. air gap)	12.30	11.70

Table 2. An abbreviated summary of fired-test results

	Rotational Speed N (rpm)	Number of turns from original gap setting*	Combustion	Maximum gage pressure (kPa)	Temperature contrast
Case A Low	1818	0	Unsatisfactory	3.6	$T_{wc} > T_{gc}$
	2800	3	Unsatisfactory	7.8	$T_{wc} << T_{gc}$
	3888	3	Unsatisfactory	12.5	$T_{wc} << T_{gc}$
	4028	3	Unsatisfactory	12.6	$T_{wc} << T_{gc}$
Case B Medium	4690	3	Satisfactory	12.5	
	4800	3	Satisfactory	10.9	
	4902	3	Satisfactory	14.1	
	5000	0	Satisfactory	8.9	
	5000	2	Satisfactory	10.0	
	5160	3	Satisfactory	13.1	$T_{wc} < T_{gc}$
	5180-I	1	Satisfactory	9.1	For all runs in this group except those runs marked by **
	5180-II	1	Satisfactory	13.6	
	5180	2	Satisfactory	10.1	
	5300	0	Satisfactory	8.2	
	5374	3	Satisfactory	13.5	
	5448	3	Satisfactory	11.1	
	6000	3	Satisfactory	10.5	
	6480**	3	Satisfactory	11.3	
	6880	3	Satisfactory	10.6	
	6892	3	Satisfactory	10.9	
	6902**	3	Satisfactory	11.6	
	7520**	3	Satisfactory	14.3	
Case C High	8200	3	Unsatisfactory	12.0	$T_{wc} > T_{gc}$
	8400	3	Satisfactory	15.5	$T_{wc} < T_{gc}$
	8460	3	Satisfactory	12.5	$T_{wc} < T_{gc}$
	9590	3	Unsatisfactory	13.8	$T_{wc} > T_{gc}$

* Zero represents the widest gap and three represents the narrowest gap

** For these runs, $T_{ge} > T_{gc}$

CHAPTER 6
CONCLUSIONS AND RECOMMENDATIONS

The goal of this study was to determine the performance of the prototype TurbX™ engine. This goal was successfully accomplished. The TurbX™ engine was designed by the inventor to deliver 15 kW of power at a speed of 20,000 rpm. The results are presented and discussed. The results clearly indicate that the TurbX™ engine produced no net output power for speeds up to 10,000 rpm. The temperature measurements indicated that for most of the runs there was sustained combustion. However, even in runs where satisfactory combustion was observed, measured gage pressures inside the combustion chamber never exceeded 15.5 kPa. The lack of sufficient pressure rise inside the combustion chamber is indicative of excessive leakage through the rotor/stator clearance gap in the bladed section of the rotor and further development and research are needed to address this problem.

Based on the results and the experience gained through the testing, several recommendations can be made. Some of them are relatively easy to implement without significant changes to the engine and others require significant design issues and modifications to the engine. In the order of increasing complexity, the recommendations are:

1. Install spark plugs in the combustion chambers on both stators to initiate combustion on both sides of the rotor in order to reduce or eliminate flame propagation issues and to ensure that satisfactory sustained combustion is achieved without any type of abnormal temperature variations.

2. Future testing of the engine should be done with a horizontal axis of rotation using a suitable containment shielding system.
3. Instead of methane, fuels with high-flame velocities such as hydrogen or acetylene should be used to demonstrate that this engine could develop output power. This approach bypasses the low-flame speed issues associated with methane. Once the concept is validated, the problems related to methane combustion can be addressed later. The combustion chamber should also be lengthened to allow for more time for the combustion pressure to reach a peak value.
4. Future changes should address the issues related to the reduction of the air gap between the rotor and stators, a more direct way to determine and adjust the size of the air gap, and ensure that the rotor and stator surfaces are flat and parallel.
5. The stator expansion passages should be redesigned using modern aerodynamic and computational tools to reduce pressure losses in the stators, and improve the exit angle of the flow to be compatible with the turbine blades to significantly reduce the aerodynamic impact losses. The rotor turbine blades should also be aerodynamically designed to optimally absorb the kinetic energy of the moving gas to produce work and minimize losses.

The above recommendations are primarily intended to demonstrate the feasibility of the engine. However, other issues related to the cooling of the engine are not addressed. Once the engine concept is demonstrated to be feasible, significant issues related to materials and the associated manufacturing processes will need to be addressed.

LIST OF REFERENCES

LIST OF REFERENCES

1. Wilson, Michael W., *"Efficiency Enhanced Turbine Engine."* US Patent Number 5,966,927, October 19, 1999.

2. Wilson, Michael W., *"Efficiency Enhanced Turbine Engine."* US Patent Number 6,105,359, August 22, 2000

3. Thesis, T.J., Conklin, J.C., Thomas, J.F., Armstrong, T.R., "*Comparison of Prime Movers Suitable for USMC Expeditionary Power Sources.*" ORNL/TM-2000/116, Oak Ridge National Laboratory March 2000.

4. Dey, N.C., *"Heat Engines and Applied Thermodynamics."* Asia Publishing House, New York, 1964.

5. Obert, Edward F., *"Internal Combustion and Air Pollution."* Harper & Row Publishers, Inc., New York, 1973.

6. Venturini, Osvaldo Jose, and Varella, Sebastiao, "*A Reevaluation of the Holzwarth Gas Turbine Cycle for Use in Small Power Plants.*" ASME Paper 2001-GT-547, International Gas Turbine & Aeroengine Congress & Exhibition, New Orleans, USA, June 2001.

7. SolidWorks® 97Plus, SolidWorks Corporation, Concord Massachusetts, 1997.

8. Turns, Stephen R., *"An Introduction to Combustion. Concepts and Applications."* McGraw Hill Companies, Inc., Boston, 2000.

9. Kuo, Kenneth K., *"Principles of Combustion"*, Johnson Wiley & Sons, Inc., New York, 1986.

APPENDICES

APPENDIX A

TEMPERATURE ABNORMALITIES ($T_{wc} > T_{gc}$)

In the two test runs at 8200 and 9590 rpm shown in Figures 34 and 37, all three thermocouples measured temperature rises of less than about 80°C, indicating unsatisfactory combustion. In these runs it can also be seen that the wall temperature inside the combustion chamber (T_{wc}) is found to be greater than gas temperature inside the combustion chamber (T_{gc}) throughout the entire fuel injection time interval. This is abnormal because the gases should be heating the walls and not the other way around. This abnormality ($T_{wc} > T_{gc}$) can be explained by considering rotational speed of the rotor and methane flame speeds shown in Tables A.1 and A.2.

To illustrate the proposed explanations for this abnormality, calculations were performed showing the tangential velocity of the rotor relative to the flame speed for methane. Table A.1 shows the ranges of laminar and turbulent flame speeds of methane-air mixtures. The laminar range of flame speeds correspond to lean to stoichiometric mixture conditions. The turbulent flame speed range corresponds to minimum-to-maximum turbulent intensities of the flame.

Table A.1. Premixed flame speeds of methane-air mixtures at atmospheric pressure

	Laminar Flame Speed (cm/s)	Turbulent Flame Speed (cm/s)	Source
1.	≈15-40	≈150-1500	[8]
2.	≈27-37	-	[9]

Table A.2. Tangential rotor velocity relative to methane flame velocities

Rotor Speed (rpm)	Tangential Rotor Velocity (cm/s)	Ratio of Rotor Velocity to Minimum Laminar Flame Speed	Ratio of Rotor Velocity to Maximum Laminar Flame Speed	Ratio of Rotor Velocity to Minimum Turbulent Flame Speed	Ratio of Rotor Velocity to Maximum Turbulent Flame Speed
1818	818.6	54.6	20.5	5.5	0.5
8200	3692.4	246.1	92.3	24.6	2.5
9590	4318.3	287.9	107.8	28.8	2.9

Table A.2 shows the ratios of tangential velocity of the rotor to the laminar flame speed and turbulent flame speed. For the two higher speeds (8200 and 9590 rpm) the results in Table A.2 indicate the rotor speed is approximately 2.5 times greater than the maximum turbulent flame speed.

It can be seen that the flame velocity is smaller relative to rotor speed and, therefore, the flame is unlikely to penetrate across rotor turbine blades to the combustion chamber located across the rotor on the opposite stator where the T_{gc} thermocouple is located. As the flame propagates outward from the source of ignition and reaches the rotor, the rotor sweeps the flame downstream preventing it from reaching T_{gc} thermocouple. Therefore, the hot combustion gases that are being swept downstream toward the region where T_{wc} thermocouple is located would be exposed to higher temperatures than T_{gc} thermocouple that is located upstream in the combustion chamber. Except for the case of maximum turbulent flame speed, the above explanation is also applicable for the engine speed of 1818 rpm.

APPENDIX B

TEMPERATURE ABNORMALITIES ($T_{ge} > T_{gc}$)

In test runs at 6480, 6902 and 7520 rpm shown in Figures 29, 32 and 33 it can be seen that (1) during for the first 30-seconds to one-minute of fuel injection the maximum temperatures were under about 150°C indicating unsatisfactory combustion, and during this period (2) the gas temperature in the last expansion stator passage (T_{ge}) is found to have exceeded the gas temperatures inside the combustion chamber (T_{gc}). This temperature abnormality is unexpected because the temperature of hot combustion gases should decrease as the gas expands through the stator expansion passages especially because the last expansion passage is farthest from the combustion chamber.

A possible explanation for this temperature abnormality ($T_{ge} > T_{gc}$) is as follows. During the start of a run, as the fuel flow rate to TurbX™ is increased, the fuel-air ratio of the mixture increases from zero to a final stoichiometric value. During this time interval, since the airflow rate remains constant, the air-fuel mixture varies from very lean state to a stoichiometric state. For hydrocarbon fuels the flame velocities decrease from their peak values at stoichiometric or slightly fuel-rich mixtures [9]. Therefore, the fuel-lean conditions will delay combustion inside the combustion chamber and the fuel will continue to burn into the stator expansion passages resulting in the T_{ge} thermocouple measuring about 15°C higher than the gas temperatures inside the combustion chamber (T_{gc}).

Combustion tends to be unsatisfactory when fuel flow rate is gradually increased during the first 30 to 60 seconds of the fueling process. However, after this period of time, further increases in fuel flow rates resulted in T_{gc} increasing rapidly to values of 500°C indicating satisfactory combustion.

VITA

Kurt Erickson was born in Logan, Utah on May 18, 1976. Kurt attended the Cache County school system, in Logan, Utah where he graduated from Logan High School in the spring of 1994. From there, he went to Utah State University and received a Bachelor of Science in Mechanical Engineering in the spring of 2000. After completing his undergraduate study he married Nicole Miller of Highland, Utah. After graduation, he and his wife decided to take on a big adventure and to move to Knoxville, Tennessee where he continued to pursue his education to receive a Master of Science degree in Mechanical Engineering at the University of Tennessee, Knoxville. He will receive his Master of Science degree in Mechanical Engineering in the summer of 2002.